Pharm Res
DOI 10.1007/s11095-017-2271-7

RESEARCH PAPER

A Novel Phenylchromane Derivative Increases the Rate of Glucose Uptake in L6 Myotubes and Augments Insulin Secretion from Pancreatic Beta-Cells by Activating AMPK

Naomi Rozentul[1] • Yosef Avrahami[2] • Moran Shubely[1] • Laura Levy[1] • Anna Munder[1] • Guy Cohen[2] • Erol Cerasi[3] • Shlomo Sasson[2] • Arie Gruzman[1]

Received: 27 June 2017 / Accepted: 24 September 2017

ABSTRACT

Purpose A series of novel polycyclic aromatic compounds that augment the rate of glucose uptake in L6 myotubes and increase glucose-stimulated insulin secretion from beta-cells were synthesized. Designing these molecules, we have aimed at the two main pathogenic mechanisms of T2D, deficient insulin secretion and diminished glucose clearance. The ultimate purpose of this work was to create a novel antidiabetic drug candidate with bi-functional mode of action.

Methods All presented compounds were synthesized, and characterized in house. INS-1E cells and L6 myoblasts were used for the experiments. The rate of glucose uptake, mechanism of action, level of insulin secretion and the druggability of the lead compound were studied.

Results The lead compound (6-(1,3-dithiepan-2-yl)-2-phenylchromane), dose- and time-dependently at the low μM range increased the rate of glucose uptake in L6 myotubes and insulin secretion in INS-1E cells. The compound exerted its effects through the activation of the LKB1 (Liver Kinase B1)-AMPK pathway. *In vitro* metabolic parameters of this lead compound exhibited good druggability.

Conclusions We anticipate that bi-functionality (increased rate of glucose uptake and augmented insulin secretion) will allow the lead compound to be a starting point for the development of a novel class of antidiabetic drugs.

KEY WORDS AMPK activation · glucose uptake · insulin secretion · LKB1 activation · phenylchromane scaffold

ABBREVIATIONS

[^{3}H]dGlc	1-Tritium-2-deoxyglucose
ACC	Acetyl-CoA carboxylase
AICAR	5-Aminoimidazole-4-carboxamide-1-β-D-ribofuranoside
Akt/PKB	Akt/Protein kinase B
AMPK	AMP kinase
AS160	AMPK substrate of phosphorylation 160 kDA
BDA	Benzaldehyde dimethyl acetal
CYP	Cytochrome P450
DCM	Dichloromethane
DEAD	Diethyl azodicarboxylate
DMF	Dimethrylformamide
GLUT4	Glucose transporter type 4
GSIS	Glucose-stimulated insulin secretion
hERG	"Human ether-à-go-go"-related gene channels
HRP	Horseradish peroxidase
LKB1	Liver Kinase B1
mGPD	Mitochondrial glycerophosphate dehydrogenase
OPD	O-phenylenediamine

Naomi Rozentul and Yosef Avrahami contributed equally to this work.

Electronic supplementary material The online version of this article (https://doi.org/10.1007/s11095-017-2271-7) contains supplementary material, which is available to authorized users.

✉ Shlomo Sasson
shlomo.sasson@mail.huji.ac.il

✉ Arie Gruzman
gruzmaa@biu.ac.il

[1] Division of Medicinal Chemistry, Department of Chemistry, Faculty of Exact Sciences, Bar-Ilan University, 52900 Ramat-Gan, Israel

[2] Department of Pharmacology, Institute for Drug Research, School of Pharmacy, Faculty of Medicine, The Hebrew University of Jerusalem, 91120 Jerusalem, Israel

[3] The Endocrinology and Metabolism Service, Department of Medicine Hadassah-Hebrew University Medical Center, 91120 Jerusalem, Israel

Published online: 05 October 2017

PCC	Pyridinium Chlorochromate
PMSF	Phenylmethanesulfonylfluoride
QTof	Quadrupole time of-flight mass spectrometer
T2D	Type 2 diabetes
THF	Tetrahydrofuran
TMS	Tetramethylsilane
TMSCl	Trimethylsilyl chloride
TosCl	Toluenesulfonyl chloride

INTRODUCTION

Despite recent intensive efforts to find a cure and/or optimal treatment for type 2 diabetes (T2D), the almost one-century old metformin remains the first-line oral antidiabetic drug (1). However, metformin is not an ideal drug: although it is well-tolerated by patients and exerts efficient blood glucose lowering effect, normoglycemia is not restored, and it does not prevent all late complications of diabetes (2). Therefore, the need for novel, more effective and potent antidiabetic drugs is still intense.

Skeletal muscles are the main consumers of glucose (3). During exercise or upon insulin stimulation glucose transporter type 4 (GLUT4) translocates from the cytoplasm to the sarcolemma and T-tubules, thus, augmenting the rate of glucose influx, and consequently lowering blood glucose levels (4). T2D patients suffer from insulin-resistance in skeletal muscles; however this does not affect contraction-mediated GLUT4 recruitment from intracellular storage compartments to the plasma membrane (5). This pathway is regulated by the key energy sensor enzyme AMPK (6–8). LKB1 is a major upstream stimulatory kinase that phosphorylates the α-subunit of AMPK at Thr172 (9,10). Several compounds, such as berberine (11), silibinin (12) and ursolic acid (13) were shown to have beneficial effects on glucose and lipid homeostasis by activating LKB1. Yet, other molecules show similar effects by direct activation of AMPK and not its upstream regulator LKB1 (14–16). It is suggested that metformin exerts its pharmacological effects by activating AMPK; yet, other mechanisms were also proposed. For example, inhibition of gluconeogenic gene expression and allosteric regulation of key gluconeogenesis enzymes in the liver, direct regulation of miRNAs, which modulate several downstream genes in metabolic or preoncogenic pathways (17,18). Also, direct inhibition of mGPD (mitochondrial glycerophosphate dehydrogenase), resulting in altered cellular redox state (19) was proposed as metformin's mechanism of action. Direct activators of AMPK such as A769662, PT-1, 5-aminoimidazole-4-carboxamide-1-β-D-ribofuranoside (AICAR), 2-(benzo[d]thiazol-2-ylmethylthio)-6-ethoxybenzo[d]thiazole and others, have been discovered or synthesized, but none could be developed into antidiabetic drugs (4,14,15,20–24). The fact that exercise is a potent stimulus for increasing skeletal muscle GLUT4 expression, trafficking and glucose uptake in a non-insulin-dependent manner (25) supports the hypothesis that AMPK activation should be a major target for designing novel and potent antidiabetic drugs (14,26,27).

LKB1 controls several key functions also in beta-cells (28)], which are related to morphological characteristics such as polarity, cell size and total beta-cell mass in islets of Langerhans (29). Glucose-stimulated insulin secretion (GSIS) may also be regulated by this kinase (29,30). Several studies reported that LKB1 activation downregulated insulin secretion (31–33). Studies on the activation of AMPK in beta-cells also produced conflicting results (34,35). Some showed that AMPK activation decreased insulin secretion and promoted apoptosis (36–38), while others attested to opposite effects (39–41). For example, AMPK activators increased GSIS from rat insulinoma cells and isolated rat islets (42). Moreover, mice lacking or expressing inactive AMPK forms in beta-cells exhibited augmented peripheral insulin sensitivity and limited GSIS capacity that was associated with pathological alterations in beta-cell morphology (43). The reason for these conflicting results is not clear, and can be attributed to different *in vitro* and *in vivo* biological models that were used in these studies..

In our previous studies we showed that D-xylose derivatives (3-O-methyl- 2,4-benzylidene-D-xylose diethyl dithioacetal, 2,4-benzylidene-D-xylose diethyl dithioacetal, 2,4:3,5-dibenzylidene-D-xylose diethyl dithioacetal) augmented glucose uptake in skeletal muscles in a non-insulin-dependent manner by activating AMPK (44,45). In addition, using molecular modelling we also designed and synthesized two AMPK activators based on the benzothiazole core; 2-(benzo[d]thiazol-2-ylmethylthio)-6-ethoxybenzo[d]thiazole and 2-(propylthio)benzo-[d]thiazol-6-ol These compounds stimulated glucose uptake in skeletal muscles and also increased GSIS from cultured beta-cells and isolated rat islets of Langerhans: (42,46). However, all these compounds were protected under different patents. Thus, to accelerate the drug development process and to interest pharmaceutical companies, we developed novel, patentable compounds, which belong to a new class of bi-functional AMPK activators. In this work we show that molecules with a phenylchromane core augmented glucose uptake in myotubes and increased GSIS from beta-cells.

MATERIALS AND METHODS

Organic solvents (HPLC grade) were from Frutarom Ltd. (Haifa, Israel). Dry THF was obtained using distillation from a boiled blue color mix with sodium/benzophenone. The melting points were determined with Fisher-Johns melting point apparatus (Palmerton, PA). The ^{1}H NMR and ^{13}C NMR spectra were recorded at room temperature on a Bruker Advance NMR spectrometer (Vernon Hills, IL)

operating at 200 and 300 MHz and were in accord with the assigned structures. Chemical shift values were reported relative to TMS that was used as an internal standard. The samples were prepared by dissolving the synthesized compounds in DMSO-d6 (δH = 2.50 ppm, δC = 39.52 ppm) or in $CDCl_3$ (δH = 7.26 ppm, δC = 77.16 ppm) (47). Chemical shifts were expressed in δ (ppm) and coupling constants (J) in hertz. The splitting pattern abbreviations are as follows: s, singlet; d, doublet; t, triplet; q, quartet; quint, quintet; m, unresolved multiplet due to the field strength of the instrument; dd, doublet of doublet. A QTof micro spectrometer (Micromass, Milford, MA) in the positive ion mode was used for mass spectrometry. Data were processed using massLynX v.4.1 calculation and deconvolution software (Waters Corporation, Milford, MA). Column chromatography was performed on Merck Silica gel 60 (230–400 mesh; Merck, Darmstadt, Germany). Analytical and preparative HPLC (Young Lin Instruments, Anyang, Korea) were performed on LUNA C18(2) preparative (10 μm, 100 x 30 mm) or analytical (5 μm, 250 x 4.6 mm) columns, both from Phenomenex Inc. (Torrance, CA). Acetonitrile and doubly distilled water were used as an eluent in different ratios. Analytical thin layer chromatography was carried out on pre-coated Merck Silica gel 60F254 (Merck) sheets using UV absorption and iodine physical adsorption for visualization. The ≥95% purity of the final compounds was confirmed using HPLC analysis. All analytical data (including the NMR images) is shown in Supportive Information. Human insulin (Actrapid) was purchased from Novo Nordisk (Bagsvaerd, Denmark). AICAR, BSA, 2-deoxy-D-glucose (dGlc), D-glucose, O-phenylenediamine (OPD), and the protease inhibitor cocktail were purchased from Sigma-Aldrich Chemicals (Rehovot, Israel). Glycerol and sodium fluoride were from Merck (Whitehouse Station, NJ). Mercaptoethanol, phenylmethanesulfonylfluoride (PMSF), sodium orthovanadate, sodium-β-glycerophosphate, sodium pyrophosphate and SDS were purchased from Alfa Aesar (Ward Hill, MA). American Radiolabeled Chemicals (St. Louis, MO) supplied [^{3}H]dGlc [2.22 TBq/mmol (60 Ci/mmol)]. Antibodies against AMPKα, pThr172-AMPK, LKB1, pSer438-LKB1, pSer437-AKT, ACC, pSer79-ACC AS-160 and pThr642-AS160 were purchased from Cell Signaling Technology (Beverly, MD). The α-tubulin was from Millipore (Billerica, MA). The Anti-c-Myc (A-14) antibody was from Santa Cruz Biotechnology (Santa Cruz, CA), horseradish peroxidase (HRP)-conjugated anti-rabbit IgG and EZ-ECL chemoluminescence detection kit were from Jackson ImmunoResearch (West Grove, PA). Goat serum, fetal calf serum (FCS), L-glutamine, α-minimal essential medium (MEM) and antibiotics were purchased from Biological Industries (Beth-Haemek, Israel). P450-Glo™ Assay Systems was purchased from Promega (Madison, WI, USA). PredictorTM hERG Fluorescence Polarization Assay kit was purchased from Invitrogen (Carlsbad, CA, USA).

SYNTHETIC PROCEDURES

3-chloro-1-phenylpropan-1-one (**I**) was synthesized as described (48).

The title compound was obtained starting from 3-chloropropionyl chloride (yellow oil, 70%): ^{1}H NMR (200 MHz, $CDCl_3$): δ = 3.45 (t, J = 6.8 Hz, 2H), 3.92 (t, J = 6.8 Hz, 2H), 7.47 (m, 2H), 7.59 (m, ^{1}H), 7.93 ppm (m, 2H); ^{13}C NMR (50.32 MHz, $CDCl_3$): δ = 38.71, 41.32, 128.08, 128.78, 133.59, 136.40, 196.74 ppm; MS (ESI) m/z: 169 [M + H].

3-chloro-1-phenylpropan-1-ol (**2**) was synthesized as described (48).

The title compound was obtained starting from **I** (yellow oil, 97%): ^{1}H NMR (200 MHz, $CDCl_3$): δ = 2.05 (m, 1H), 2.20 (m, 1H), 3.51 (m, 1H), 3.68 (m, 1H), 4.88 (q, J = 4.8 Hz, 1H), 7.32 ppm (m, 5H); ^{13}C NMR (50.32 MHz, $CDCl_3$): δ = 41.29, 41.58, 71.15, 125.64, 127.76, 128.51, 143.55 ppm; MS (CI) m/z: 171 [M + H].

1-(3-chloro-1-phenylpropoxy)-2, 4-dibromobenzene (**3**) was synthesized as described (49).

The title compound was obtained starting from **2** (white solid, 54%): ^{1}H NMR (300 MHz, $CDCl_3$): δ = 2.24 (m, 1H), 2.53 (m, 1H), 3.64 (m, 1H), 3.89 (m, 1H), 5.39 (q, J = 4.5 Hz, 1H), 6.57 (d, J = 9 Hz, 1H), 7.15 (dd, J = 9 Hz, J = 3 Hz, 1H), 7.34 (m, 5H), 7.64 ppm (d, J = 3 Hz, 1H); ^{13}C NMR (75.49 MHz, $CDCl_3$): δ = 41.24, 78.22, 113.32, 113.59, 116.23, 125.88, 128.33, 128.99, 131.06, 135.49, 139.67, 153.47 ppm; MS (ESI) m/z: 404 [M].

3, 4-dihydro-2-phenyl-2H-chromene-6-carbaldehyde (**4**) was synthesized as described (50).

The title compound was obtained starting from **3** (yellow solid, 25%): ^{1}H NMR (300 MHz, $CDCl_3$): δ = 2.28 (m, 2H), 2.90 (m, 1H), 3.04 (m, 1H), 5.17 (q, J = 3 Hz, 1H), 7.02 (d, J = 8.4 Hz, 1H), 7.40 (m, 5H), 7.66 (m, 2H), 9.86 ppm (s, 1H); ^{13}C NMR (75.49 MHz, $CDCl_3$): δ = 41.23, 41.32, 116.29, 126.02, 128.48, 129.20, 130.30, 132.06, 139.95, 163.08, 190.93 ppm; MS (ESI) m/z: 239 [M + H].

General Procedure for the Preparation of (**5**, **6**, **7**, **8**, **9**, **12**, **13**, **14**, **15**, **19**) (51).

To a well-stirred solution of 10 mmol of **4** or **11** and 20 mmol of corresponding thiol (or 10 mmol dithiol) in chloroform at r. t. 12–15 mmol TMSCl was added slowly over a period of 20 min. After an hour, the reaction mixture was washed with a 5% aqueous sodium carbonate solution and chloroform phase was washed by water. The organic layer was dried by Na_2SO_4, filtered and the chloroform was evaporated. The residue amorphic solids were purified by HPLC or by regular silica gel chromatography.

6-(1,3-dithian-2-yl)-2-phenylchroman (**5**):

The title compound was obtained starting from **4** (white solid, 3%): ^{1}H NMR (300 MHz, $CDCl_3$): δ = 2.02 (m, 4H), 2.85 (m, 6H), 5.16 (d, 1H), 5.64 (s, 1H), 7.33 ppm (m, 8H); ^{13}C NMR

(75.49 MHz, $CDCl_3$): δ = 25.06, 25.11, 29.82, 41.37, 57.12, 76.69, 117.06, 121.93, 126.02, 127.19, 127.82, 128.58, 129.05, 132.37, 142.60, 156.06 ppm; MS (EI) m/z: 329 [M + H].

6-(1,3-dithiolan-2-yl)-2-phenylchroman (**6**):

The title compound was obtained starting from **4** (colorless oil, 16%): ^{1}H NMR (300 MHz, $CDCl_3$): δ = 2.17 (m, 2H), 2.85 (m, 2H), 3.43 (m 4H), 5.04 (q, J = 2.7 Hz, 1H), 5.61 (s, 1H), 6.85 (d, J = 8 Hz, 1H), 7.34 ppm (m, 7H); ^{13}C NMR (75.49 MHz, $CDCl_3$): δ = 25.11, 29.86, 40.28, 56.27, 77.93, 117.05, 121.82, 126.02, 127.19, 127.92, 128.59, 129.06, 131.37, 141.60, 155.05 ppm; MS (EI) m/z: 314 [M].

6-(1,3-dithiepan-2-yl)-2-phenylchroman (**7**):

The title compound was obtained starting from **4** (white solid, 13%): ^{1}H NMR (300 MHz, $CDCl_3$): δ = 2.12 (m, 6H), 2.98 (m, 6H), 5.03 (d, J = 2.6 Hz, 1H), 5.26 (s, 1H), 6.84 (d, J = 8 Hz, 1H), 7.30 ppm (m, 7H); ^{13}C NMR (75.49 MHz, $CDCl_3$): δ = 25.11, 29.86, 31.71, 32.71, 56.67, 77.90, 117.11, 121.93, 126.01, 126.62, 127.89, 128.49, 128.56, 132.47, 141.63, 154.91 ppm; MS (EI) m/z: 342 [M].

6-(bis(ethylthio)methyl)-2-phenylchroman (**8**):

The title compound was obtained starting from **4** (colorless oil, 8%): ^{1}H NMR (300 MHz, $CDCl_3$): δ = 1.23 (t, J = 7.5, 6H), 2.15 (m, 2H), 2.51 (m, 4H), 2.85 (m, 2H), 4.88p (s, 1H), 5.04p (q, J = 2.6 Hz, 1H), 6.85 (d, J = 9 Hz, 1H), 7.16 (m, 2H), 7.35 ppm (m, 5H); ^{13}C NMR (75.49 MHz, $CDCl_3$): δ = 14.40, 25.21, 26.36, 29.93, 52.07, 77.94, 116.90, 121.91, 126.03, 126.86, 127.92, 128.58, 128.69, 132.18, 141.64, 154.79 ppm; MS (CI) m/z: 344 [M].

6-(bis(propylthio)methyl)-2-phenylchroman (**9**):

The title compound was obtained starting from **4** (yellow oil, 9%): ^{1}H NMR (300 MHz, $CDCl_3$): δ = 0.97 (t, J = 7.4 Hz, 6H), 1.59 (m, 4H), 2.13 (m, 2H), 2.52 (m, 4H), 2.78 (m, 1H), 2.98 (m, 1H), 4.82 (s, 1H), 5.04 (q, J = 2.4 Hz, 1H), 6.85 (d, J = 9 Hz, 1H), 7.18 (m, 2H), 7.36 ppm (m, 5H); ^{13}C NMR (75.49 MHz, $CDCl_3$): δ = 13.63, 22.66, 25.20, 29.92, 34.45, 52.77, 77.93, 116.86, 121.88, 126.03, 126.85, 127.91, 128.57, 128.67, 132.35, 141.65, 154.76 ppm; MS (CI) m/z: 297 [M-PrS].

General Procedure for the Preparation of (**10**) (45).

2, 6-bis (hydroxymethyl)-4-methylphenol (1 g, 5.94 mmol) was dried by three washes with toluene and evaporation. It was then dissolved in 10 mL of dry DMF to which 1.4 mL of BDA, 0.5 g of molecular sieve 3 Å, and 100 μL of dry hydrochloric acid 4 M (in dioxane) were added. The reaction mix was left stirring for 12 h followed by neutralization with 15% (*w*/*v*) sodium bicarbonate. The mixture was then filtered, and the filtrate was washed with chloroform, dried over $MgSO_4$, and evaporated. The residue amorphic solids were purified by HPLC, using a stepwise gradient of water and acetonitrile.

(6-methyl-2-phenyl-4H-benzo[d] [1, 3]dioxin-8-yl)methanol (**10**):

The title compound was obtained starting from 2, 6-bis (hydroxymethyl)-4-methylphenol (white solid, 35%): ^{1}H NMR (300 MHz, $CDCl_3$): δ = 2.29 (s, 3H), 4.68 (d, J = 6 Hz, 2H), 4.96 (d, J = 14.4 Hz, 1H), 5.17 (d, J = 14.4 Hz, 1H), 6.01 (s, 1H), 6.78 (s, 1H), 7.03 (s, 1H), 7.42 (m, 3H), 7.51 ppm (m, 2H); ^{13}C NMR (75.49 MHz, $CDCl_3$): δ = 20.66, 61.10, 66.73, 99.0, 124.58, 126.30, 127.89, 128.51, 129.47 ppm; MS (CI) m/z: 256 [M].

General Procedure for the Preparation of (**11**) (52).

The **10** (300 mg, 1.17 mmol) and PCC (378 mg, 1.75 mmol) in DCM (50 ml) were stirred at r. t. for 2 h. After the reaction, the mixture was purified by column chromatography (silica gel, DCM) to give pure compound **11**.

6-methyl-2-phenyl-4H-benzo[d] [1, 3]dioxin-8-carbaldehyde (**11**):

The title compound was obtained starting from **10** (white solid, 94%): ^{1}H NMR (300 MHz, $CDCl_3$): δ = 2.32 (s, 3H), 5.00 (d, J = 15 Hz, 1H), 5.20 (d, J = 15 Hz, 1H), 6.09 (s, 1H), 7.07 (m, 1H), 7.45 (m, 3H), 7.59 (m, 3H), 10.44 ppm (s, 1H); ^{13}C NMR (75.49 MHz, $CDCl_3$): δ = 20.51, 66.56, 99.39, 121.57, 123.99, 126.33, 126.95, 128.60, 129.69, 130.67, 131.72, 136.45 ppm; MS (ESI) m/z: 277 [M + Na].

8-(1,3-dithian-2-yl)-6-methyl-2-phenyl-4H-benzo[d] [1, 3]dioxin (**12**):

The title compound was obtained starting from **11** (white solid, 25%): ^{1}H NMR (300 MHz, $CDCl_3$): δ = 2.03 (m, 2H), 2.28 (s, 3H), 2.98 (m, 4H), 4.92 (d, J = 14.4 Hz, 1H), 5.12 (d, J = 14.4 Hz, 1H), 5.59 (s, 1H), 6.00 (s, 1H), 6.75 (s, 1H), 7.31 (s, 1H), 7.44 (m, 3H), 7.65 ppm (m, 2H); ^{13}C NMR (75.49 MHz, $CDCl_3$): δ = 20.64, 25.36, 32.24, 32.32, 43.05, 66.49, 99.16, 120.61, 125.34, 126.60, 126.70, 128.20, 128.44, 129.34, 130.91, 137.23, 146.98 ppm; MS (CI) m/z: 345 [M + H].

8-(1,3-dithiepan-2-yl)-6-methyl-2-phenyl-4H-benzo[*d*] [1, 3]dioxin (**13**):

The title compound was obtained starting from **11** (white solid, 11%): ^{1}H NMR (300 MHz, $CDCl_3$): δ = 2.09 (m, 4H), 2.28 (s, 4H), 2.85 (m, 2H), 3.12 (m, 2H), 4.93 (d, J = 14.4 Hz, 1H), 5.13 (d, J = 14.4 Hz, 1H), 5.70 (s, 1H), 6.01 (s, 1H), 6.73 (s, 1H), 7.33 (s, 1H), 7.44 (m, 3H), 7.62 ppm (m, 2H); ^{13}C NMR (75.49 MHz, $CDCl_3$): δ = 19.70, 30.61, 30.67, 31.56, 47.52, 65.48, 97.96, 123.81, 125.43, 126.61, 127.36, 128.22 ppm; MS (EI) m/z: 358 [M].

8-(1,3-dithiolan-2-yl)-6-methyl-2-phenyl-4H-benzo[*d*] [1, 3]dioxin (**14**):

The title compound was obtained starting from **11** (white solid, 23%): ^{1}H NMR (300 MHz, $CDCl_3$): δ = 2.29 (s, 3H), 3.38 (m, 4H), 4.94 (d, J = 14.4 Hz, 1H), 5.15 (d, J = 14.4 Hz, 1H), 6.01 (s, 1H), 6.74 (s, 1H), 7.43 (m, 4H), 7.63 ppm (m, 2H); ^{13}C NMR (75.49 MHz, $CDCl_3$): δ = 20.91, 39.54, 39.63, 48.37, 66.65, 99.04, 120.49, 124.75, 126.45, 127.25, 128.47, 128.74, 129.37, 130.51, 137.11 ppm; MS (EI) m/z: 330 [M].

8-(bis(ethylthio)methyl)-6-methyl-2-phenyl-4H-benzo[*d*] [1, 3]dioxin (**15**):

The title compound was obtained starting from **11** (white solid, 26%): ^{1}H NMR (300 MHz, $CDCl_3$): δ = 1.22 (m, 6H),

2.29 (s, 3H), 2.58 (m, 4H), 4.95 (d, J = 14.4 Hz, 1H), 5.15 (d, J = 14.4 Hz, 1H), 5.42 (s, 1H), 5.98 (s, 1H), 6.73 (s, 1H), 7.33 (s, 1H), 7.43 (m, 3H), 7.59 ppm (m, 2H); ^{13}C NMR (75.49 MHz, $CDCl_3$): δ = 14.44, 20.87, 26.46, 26.49, 43.66, 66.72, 99.11, 120.36, 124.62, 126.37, 127.68, 128.47, 129.39, 130.84, 137.21, 147.25 ppm; MS (ESI) m/z: 383 [M + Na], 399 [M + K].

General Procedure for the preparation of (**16**) (53).

2,2– dimethyl– 1,3- propanediol (10 g, 0.096 mol) dissolved in 21 ml of pyridine was added during 30 min to a stirred solution of p- toluenesulfonyl chloride (55 g, 0.288 mol) in 70 ml of DCM, maintained at 14–18°C. The reaction mixture was stored at 0°C for 4 days, filtered free from pyridine hydrochloride, and washed well with diluted HCl, and then with diluted $NaHCO_3$ solution. The solvent was removed by distillation and the viscous residue was warmed briefly under a vacuum and then poured into vigorously stirred petroleum ether to precipitate a crystalline product. Recrystallization from isopropyl alcohol gave pure product.

2, 2-dimethylpropane-1, 3-diylbis (4-methylbenzenesulfonate) (**16**):

The title compound was obtained starting from 2,2– dimethyl– 1,3- propanediol (white solid, 69%): ^{1}H NMR (300 MHz, $CDCl_3$): δ = 0.88 (s, 6H), 2.46 (s, 6H), 3.71 (s, 4H), 7.35 (d, J = 8 Hz, 4H), 7.74 ppm (d, J = 8 Hz, 4H); ^{13}C NMR (75.49 MHz, $CDCl_3$): δ = 21.06, 21.70, 35.40, 73.74, 127.92, 129.98, 132.52, 145.03 ppm; MS (ESI) m/z: 413 [M + H], 435 [M + Na], 472 [M + K].

General Procedure for the preparation of (**17**) (54).

16 (2 g, 4.85 mmol) and KSCN (11.5 g, 118.34 mmol) were stirred in dry DMF (40 mL) at 125°C for 12 h under nitrogen. Most of the solvent was removed under reduced pressure on hot to produce a brownish paste. Water (50 mL) was added to the paste and the mixture was extracted with ethyl acetate (4 × 100 mL). The organic layer was dried over Na_2SO_4 and concentrated under reduced pressure.

2, 2-dimethyl-1,3-dithiocyanatopropane (**17**):

The title compound was obtained starting from 16 (yellow oil, 100%): ^{1}H NMR (300 MHz, $CDCl_3$): δ = 1.24 (s, 6H), 3.09 ppm (s, 4H); ^{13}C NMR (75.49 MHz, $CDCl_3$): δ = 24.81, 37.40, 43.98, 111.86 ppm; MS (CI) m/z: 187 [M + H].

2, 2 -dimethylpropane-1,3-dithiol (**18**) was synthesized as described (54).

The title compound was obtained starting from **17** (yellow oil, 18%): ^{1}H NMR (300 MHz, $CDCl_3$): δ = 0.99 (s, 6H), 2.04 (s, 1H), 2.52 (s, 2H), 2.55 ppm (s, 2H); MS (EI) m/z: 136 [M].

8-(5,5-dimethyl-1,3-dithian-2-yl)-6-methyl-2-phenyl-4H-benzo[d] [1, 3]dioxin (**19**) (51).

The title compound was obtained starting from **11** and **18** (white solid, 44%): ^{1}H NMR (300 MHz, $CDCl_3$): δ = 1.10 (s, 3H), 1.38 (s, 3H), 2.29 (s, 3H), 2.45 (d, J = 14 Hz, 2H), 2.99 (d, J = 14 Hz, 2H), 4.92 (d, J = 14.4 Hz, 1H), 5.12 (d, J = 14.4 Hz, 1H), 5.44 (s, 1H), 5.99 (s, 1H), 6.75 (s, 1H), 7.39 (s, 1H), 7.44 (m, 3H), 7.63 ppm (m, 2H); ^{13}C NMR (75.49 MHz, $CDCl_3$): δ = 20.72, 23.33, 25.85, 31.22, 43.20, 44.52, 44.58, 66.56, 99.19, 120.64, 122.52, 125.34, 126.65, 128.12, 128.47, 129.38, 130.84, 134.49 ppm; MS (EI) m/z: 372 [M].

Cell Cultures

INS-1E cells were grown as previously described (42). L6 myoblasts were grown and let to differentiate into myotube as previously described (55,56). Human embryonic kidney cells (HEK 293) were maintained as described (57).

Isolation of Mononuclear Cells from Human Peripheral Blood by Density Gradient Centrifugation

Mononuclear cells were isolated from human peripheral blood by the Ficoll-based protocol developed by Sanderson *et al.* (58). Briefly, 20 ml of the whole blood was withdrawn from a healthy donor under sterile conditions. The blood was diluted 1:1 with warm PBS.. Ficoll-Paque solution was added to the diluted blood at a 3:4the ratio. Following centrifugation at 470xg (~1500 rpm) for 35 min at 20°C in a swinging bucket rotor without brake, the upper layer containing plasma and platelets was removed, leaving the mononuclear cell layer undisturbed at the interface. This layer was removed and mixed with cold sterile PBS (30 mland centrifuged at 4°C for 5 min at 400xg (1000 rpm). The resulting pellet was resuspended in seeding media (RPMI 1640, 10% FCS, 1% L-glutamine and seeded ($2x10^6$ cells/well in 6-well plates). Cells were incubated overnight before the common Trypan blue toxicity assay.

Measurement of dGlc Uptake

The rate of [^{3}H]dGlc uptake in myotubes in the absence or presence of insulin was measured as described [42]. Briefly, L6 myotubes cultures were usually preincubated in α-MEM supplemented with 2% (*v*/v) FCS and 23.0 mM D-glucose for 24 h, after which they were treated as described in each experiment The cultures were then rinsed 3 times with PBS at room temperature and further incubated with PBS, pH 7.4, containing 0.1 mM dGlc and 1.3 μCi/mL [^{3}H]dGlc for 5 min at room temperature. The uptake was stopped by 3 rapid washes with ice-cold PBS. The myotubes were then lysed with 0.1% (*w*/*v*) SDS in water and taken for liquid scintillation counting of tritium.

MTT Assay

In order to determine the toxicity of the test compound, L6 myoblasts or INS-1E cells (10,000 cells/well) were plated in 96-well tissue culture plates in 0.1 mL of the culture medium and incubated overnight. The medium was then replaced with fresh medium containing a serial dilution of tested

compounds starting up to 100 μM. HEK293 cells were incubated with 50 μM of compound 7. Following 24 h incubation of the plates at 37°C, the cell survival was determined by MTT assay, as described (59).

Western Blot Analyses

Whole-cell lysates were prepared in the following manner: the cells were washed with ice-cold PBS, and 1 mL lysis buffer was then added and incubated at 4°C for 40 min. The lysis buffer contained 50 mm Tris·HCl, pH 7.5, 1 mm EDTA, 1 mm EGTA, 1 mm Na_3VO_4, 150 mm NaCl, 50 mm NaF,10 mm sodium glycerophosphate, 5 mm sodium pyrophosphate, and 1 mm PMSF, supplemented with 0.1% (*v*/v) NP-40, 0.1% (v/v) β-mercaptoethanol, and protease inhibitor cocktail (1:100 dilution). The resulting cell lysates were centrifuged at 8700 g for 30 min at 4°C and the resulting supernatant fractions were separated and kept at -80°C until use. Protein content in the supernatant was determined according to the Bradford assay, using a BSA standard dissolved in the same buffer. Aliquots (5–60 μg) were mixed with the sample buffer [62.5 mM Tris·HCl, pH 6.8, 2% (*w*/*v*) SDS, 10% (*v*/v) glycerol, 50 mm DTT, and 0.01% (w/v) bromophenol blue] and heated at 95°C for 5 min. The proteins were then separated by 10% SDS-PAGE and Western blot detection were performed according to suppliers' protocols for the different antibodies against AMPKα, pThr172-AMPKα, Akt, pSer473-AKT, AS160, pThr642-AS160, LKB1, pSer428-LKB1, ACC pSer79-ACC and GLUT4 (Cell Signaling Technology, Beverly, MA). Bands were visualized with ECL plus (GE solution Biosciences, Pittsburgh, PA, USA) and scanned in BioRad ChemiDoc XRS + Gel Imaging system, Hercules, CA). The band density was evaluated by the Image Quant program (GE Healthcare, Chicago, IL).

GLUT4myc Plasma Membrane Content Measurement in L6 Myotubes

The colorimetric detection of surface GLUT4myc in L6 myotubes was performed as described (60). Briefly, cultured myotubes were incubated with rabbit anti-c-Myc antibody (1:200 dilution; Santa Cruz Biotechnology, Santa Cruz, CA), washed and fixed with 3% formaldehyde, and further interacted with goat HRP-conjugated anti-rabbit IgG (1:2000 dilution, Santa Cruz Biotechnology, USA). Following the washes, a solution of OPD (o-phenilendiamine) was added, and the culture plates were taken for absorbance measurement at 492 nm to estimate the relative abundance of GLUT4myc on the plasma membrane of the myotubes. The GLUT4myc L6 cells were the courtesy of Dr. A. Klip, Hospital for Sick Children (Toronto, ON, Canada).

AMPK Silencing with shRNA

Subconfluent L6 myoblasts cultures were transfected with Lentivirus consisting harboring shRNA against rat AMPKα2 (courtesy of Dr. Rachel Hertz (Department of Human Nutrition and Metabolism, The Hebrew University Faculty of Medicine, Jerusalem, Israel) and used as described by Za'tara C., *et al.* (61). Cells were harvested 72 h after transfection and treatments, and lysates were prepared and used for Western blot analyses.

GSIS

The assays were performed for INS-1E medium and lysates as previously described using Insulin ELISA kit (Merck Millipore, Billerica, MA) (62).

Measurement of hERG Function

The experiment was performed using PredictorTM hERG Fluorescence Polarization Assay kit in accordance with the manufacturer's protocol (Protocol PV5365, available online: http://tools.invitrogen.com/content/sfs/manuals/Predictor_hERG_FP_Assay_man.pdf). Fluorescence Polarization (FP) measurement is based on the observation that when a small fluorescent molecule (tracer) is excited by the polarized light, the emitted light is largely depolarized because of the rapid rotation of the molecule in the solution. The FP measurement was performed by incubating the tracer and membranes with hERG channel for 2–4 h in the buffer. The maximal fluorescence polarization was detected with no interference in the interaction between the tracer and (minimal tracer rotation). However, when test compounds (i.e., **7**) compete with the tracer for the interaction with hERG channel, the polarization of the emitted light decreases due to the ability of free unbound tracer to rotate rapidly in the buffer. The degree of binding between a test compound and hERG is proportional to the decreasing signal. The reference compound (E-4031, provided by the manufacturer) was used as a control. To compare the IC50 value of E-4031 in the assay with the data provided by the manufacturer, dose-response curve of the E-4031 was generated. Three concentrations of the test compound were used, 1, 5 μM and 25 μM ($n = 3$). Reference inhibitor (E-4031) was used at 30 μM as recommended by the manufacturer.

Measurement of P450 Activity

The experiment was performed using P450-Glo™ Assay Systems (Promega, Madison, WI, United States) in accordance with the manufacturer's protocols. The P450-Glo™

Assays provide a luminescent readout-based method for measuring cytochrome P450 activity. A conventional cytochrome P450 reaction is performed by incubating recombinant cytochrome P450 and a luminogenic cytochrome P450 substrate. The substrates in the P450-Glo™ assays are derivatives of beetle luciferin. The derivatives themselves are not substrates for luciferase but are converted by cytochrome P450 isotypes to luciferin, which in turn reacts with luciferase to produce light. The amount of light produced is directly proportional to the cytochrome P450 activity. All test points were performed in quadruplicates. Control membranes without enzymes represent the negative control (baseline). Final DMSO concentration in the reaction mixtures was 0.25%. The list of the reference compounds and their concentrations are listed in Suppl. Table 2. Test concentrations of the reference compounds correspond to approximately 4-fold reported IC50 values for the corresponding cytochromes P450 (63,64), which is expected to produce nearly 100% inhibition.

Statistical Analysis

Results presented as a Mean ± SEM, statistical significance *($p < 0.05$) was calculated among experimental groups using the two-tailed Student's t-test. The QuickCalcs online service Pad Software: www.graphpad.com/quickcalcs/ttest1.cfm was used for statistical evaluations.

RESULTS AND DISCUSSION

Synthesis

We have previously discovered that compounds with a benzylidene-D-xylose diethyl dithioacetal scaffold (Chart 1) increased the rate of glucose uptake in skeletal muscles in a non-insulin-dependent manner (44,45). Presently, we have aimed at creating more effective and potent novel derivatives based on this prototype molecule. Scheme 1 describes the synthesis of such five molecules with a phenylchromane core. The Friedel–Crafts condensation between a benzene and 3-chloropropanoyl chloride was used to produce the correspondent ketone (**1**), which was further reduced to 3-chloro-1-phenylpropan-1-alcohol by $NaBH_4$ (**2**). Commercially available 2,4-dibromophenol was conjugated with **2** using the Mitsunobu reaction to obtain 2,4-dibromo-1-(3-chloro-1-phenylpropoxy)benzene (**3**). This aromatic ether was taken to intermolecular cyclization and aldehyde addition, which occurred simultaneously under extra dry conditions, in a one pot reaction, as described by Hodgetts *et al.* (50). The outcome of these reactions was the novel tricycle aldehyde 2-phenylchromane-6-carbaldehyde (**4**). This was used as a starting molecule for the synthesis of five phenylchromane-based benzylidene-D-xylose diethyl dithioacetal analogs. Formation and cleavage of thioacetals usually occurs in acid conditions under kinetic equilibrium (65). Occasionally, it

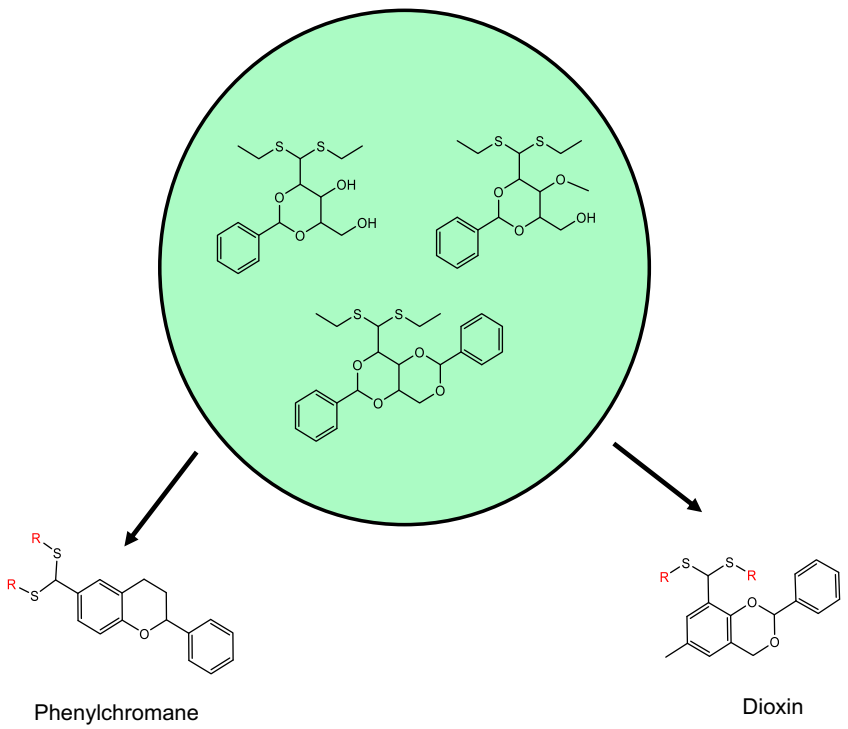

Chart 1 Two groups of synthesized compounds with phenylchromane or dioxin core.

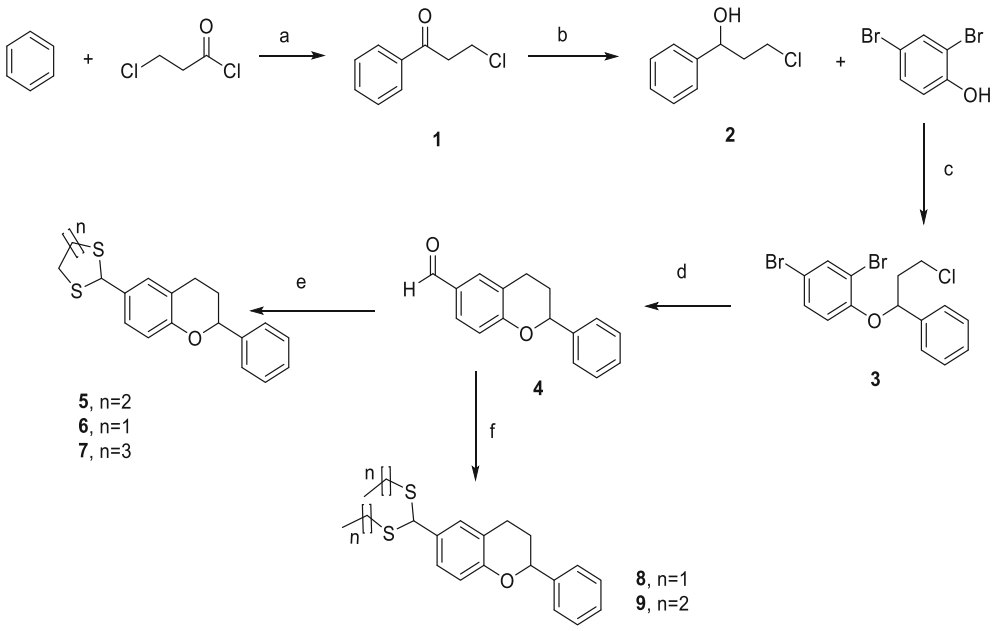

Scheme 1 Synthesis of compounds with phenylchromane core. Reagents and conditions: (**a**) $AlCl_3$, r. t., 2 h.; (**b**) $NaBH_4$, THF, r. t., 2 h.; (**c**) PPh_3, DEAD, THF, r. t., 16 h.; (**d**) n-BuLi, dry THF, dry DMF, −50° C to r. t., 2 h.; (**e**) corresponding dithiol, $CHCl_3$, TMSCl, r. t., 2 h.; (**f**) corresponding thiol, $CHCl_3$, TMSCl, r. t., 2 h.

may be difficult to define specific acidic conditions for the catalysis and formation of thioacetals while preserving their structural integrity. After several unsuccessful attempts to prepare thioacetals using **4** as a starting molecule by applying canonical methods (e.g.,, DMF with HCl) we introduced a different method to protect the hydroxyl groups (51)], which is based on gentle acidic catalysis with TMSCl. The alcohol moiety, which was not present in the reacting molecule, was formed during the thioacetal synthesis when the first thiol group attacked the aldehyde. This hydroxyl reacted with TMSCl, followed by the release of HCl, which promoted the formation of the thioacetal moiety, while the second thiol group attacked the generated cation (51). Of the seven novel thioacetals five were cyclic: 6-(1,3-dithian-2-yl)-2-phenylchromane (**5**), 6-(1,3-dithiolan-2-yl)-2-phenylchromane (6), 6-(1,3-dithiepan-2-yl)-2-phenylchromane (**7**); and two were acyclic: 6-(bis(ethylthio)methyl)-2-phenylchromane (**8**) and 6-(bis(propylthio)methyl)-2-phenylchromane (**9**). All were synthesized at room temperature using TMSCl as a catalyst together with the corresponding di- or mono- thiols,.

In addition, a second class of benzylidene-D-xylose diethyl dithioacetal analogs was synthesized. In this procedure, the 2,4-benzylidene ring was replaced by benzylmethyl domain to generate 5-methyl-2-phenyl-4H-benzo[*d*] [1, 3]dioxin core, as shown in Chart 1. The first intermediate (6-methyl-2-phenyl-4H-benzo[*d*] [1, 3]dioxin-8-yl)methanol (**10**) was synthesized under nitrogen atmosphere as described in Scheme 2. Two starting commercially available molecules, (2-hydroxy-5-methyl-1,3-phenylene)dimethanol and 1-(dimethoxymethyl)-4-methylbenzene, were coupled in the presence of a catalytic amount of HCl. The benzyl alcohol moiety in **10** was oxidized by PCC to form a novel aromatic aldehyde (**11**). The yield of the reaction was very high and close to 100%. Finally, the dithioacetal moieties were introduced to **11** by an identical procedure to the above-mentioned phenylchromane analogs method. Three different compounds that contained 5-methyl-2-phenyl-4H-benzo[*d*] [1, 3]dioxin core were synthesized: 8-(1,3-dithian-2-yl)-6-methyl-2-phenyl-4H-benzo[*d*] [1, 3]dioxin (**12**), 8-(1,3-dithiepan-2-yl)-6-methyl-2-phenyl-4H-benzo[*d*] [1, 3]dioxin (**13**), 8-(1,3-dithiolan-2-yl)-6-methyl-2-phenyl-4H-benzo[*d*] [1, 3]dioxin (**14**). The fourth product, 8-(bis(ethylthio)methyl)-6-methyl-2-phenyl-4H-benzo[*d*] [1, 3]dioxin (**15**), was the most structurally closed to the parent compound due to the presence of the dithioacetal moiety:. To obtain the fifth compound with a dioxin core, namely, 8-(5, 5-dimethyl-1, 3-dithian-2-yl)-6-methyl-2-phenyl-4H-benzo[*d*] [1, 3] dioxin (**19**), the corresponding dithiol was first synthesized as shown in Scheme 3. Two hydroxyl groups in the 2,2-dimethylpropane-1,3-diol were transformed to become good leaving groups by reactions with tosyl chloride in the presence of pyridine to obtain 2, 2-dimethylpropane-1,3-diyl bis (4-methylbenzenesulfonate) (**16**). Then, potassium thiocyanate was used as a donor of the thiocyanate groups to replace the tosyl moieties in **16**, resulting in 2, 2-dimethyl-1, 3-dithiocyanatopropane (**17**). Reduction cleavage of the thiocyanate by lithium aluminum hydride in dry THF produced the desired 2, 2-dimethylpropane-1, 3-dithiol (**18**), which was conjugated with **11** as described above.

Biological Evaluation

All synthesized compounds were first screened for their capacity to augment glucose uptake in rat L6 myotubes. This rat skeletal muscle cell-line spontaneously differentiates to multinuclear myotubes, which are morphologically similar to normal muscle myotubes (66). The compounds were tested in cultures that were

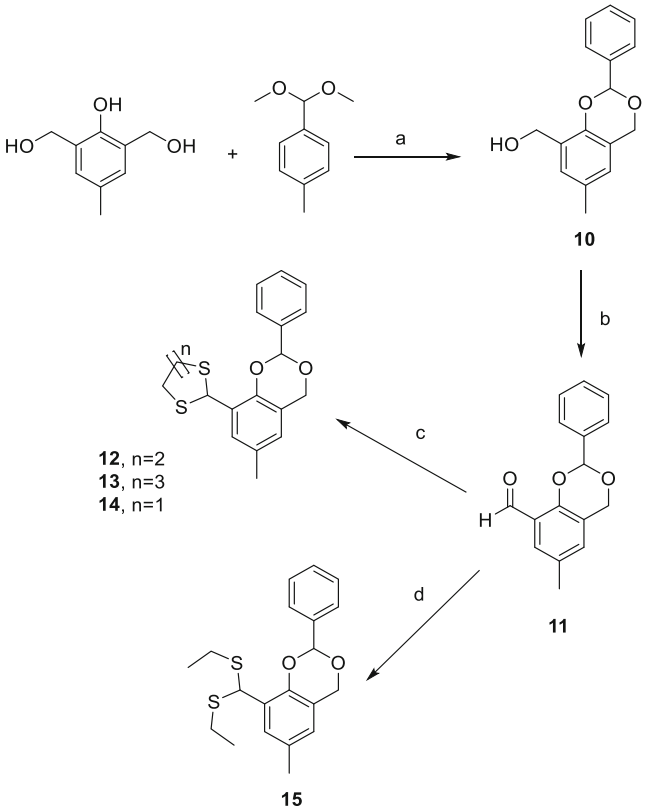

Scheme 2 Synthesis of compounds with dioxin core. Reagents and conditions: (**a**) dry DMF, molecular sieves 3Å, dry HCl in dioxane, r. t., overnight; (**b**) PCC, DCM, r. t., 2 h.; (**c**) corresponding dithiol, $CHCl_3$, TMSCl, r. t., 2 h.; (**d**) corresponding thiol, $CHCl_3$, TMSCl, r. t., 2 h.

maintained at high glucose medium (23.5 mM, to mimic hyperglycemic conditions). Under such conditions the cellular autoregulatory mechanism decreases the rate of glucose influx into the muscle (67,68). Thus, the ability of a test compound to overcome this physiological protective mechanism and to increase the rate of glucose uptake is considered a good predictor for potential antihyperglycemic effect *in vivo*.

Table 1 shows that eight out of the ten tested compounds increased moderately the rate of glucose uptake in L6 myotubes. In contrast, two compounds (**6** and **7**), both cyclic thioether 2-phenylchromane derivatives, increased the rate of glucose uptake nearly 3-fold (maximal effect), but at a relatively high concentrations (50 μM). Despite the fact that compound **15** (a dioxin derivative, the structural closest related molecule to benzylidene-D-xylose diethyl dithioacetals) had a higher potency than **7**, the latter was chosen as the lead compound and used for the biological investigation due to its higher activity (three fold stimulatory effect). Dose-response analysis of the effects of **7** on the rate of glucose uptake in L6 myotubes was performed, as shown in Fig. 1a. Already 5 μM of **7** increased significantly the rate of glucose uptake; at 10 μM **7** nearly doubled the rate of uptake; the maximal effect of **7** was observed at 50 μM (3.19-fold increase of rate of glucose uptake compared with the vehicle control). Noteworthy, at 100 μM **7** was toxic for L6 myotubes (SI Fig. 1A). Time-course analysis (Fig. 1b) shows that **7** augmented the rate of glucose uptake after a 5-h exposure. This effect gradually increased and peaked at 24-h of incubation. However, after 48 h the stimulatory effect of compound **7** decreased from 3-fold (24 h) to 1.8-fold.

Since the parent compound of **7** was an AMPK activator, we asked whether **7** shared a similar mechanism of action or mimicked insulin-induced translocation of GLUT4 (69). The ability of **7** to activate AMPK by Thr172 phosphorylating was tested at different concentrations of **7** (5, 10 and 25 μM). The Western blot analyses in Fig. 1c, d indicate that **7** increased dose-dependently the extent of AMPK phosphorylation. These analyses show that already within 3 h of incubation **7** (25 μM) increased 2-fold Thr172 phosphorylation. Comparable levels of Thr172 phosphorylation were also observed after 5 and 24 h of incubation with 25 μM of **7**. Sorbitol, a known hyperosmotic activator of AMPK, was used as a positive control in these experiments. Importantly, the time-dependent effects of **7** on glucose uptake (Fig. 1b) correlated well with the activation of AMPK (Fig. 1e, f).

Increased rate of glucose transport in skeletal muscle can result from translocation of GLUT4 from intracellular compartments to the plasma membrane or from increased intrinsic activity of the transporter (6,70–73). To test the possible effect of **7** on plasma membrane GLUT4 content, we used L6 myotubes stably expressing GLUT4myc. The cell surface expression of

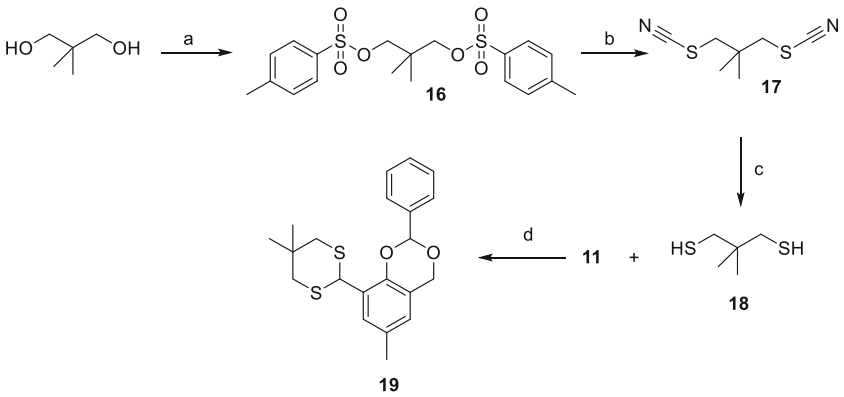

Scheme 3 Synthesis of **19**. Reagents and conditions: (**a**) TosCl, pyridine, DCM, 14–18°C; (**b**) KSCN, dry DMF, 125°C, 12 h.; (**c**) $LiAlH_4$, dry THF, 50° C, overnight; (**d**) $CHCl_3$, TMSCl, r. t., 2 h.

Table 1 Effect of tested compounds on the rate of glucose uptake in L6 myotubes

Tested compounds	Concentration	Time of maximal effect	% of activation ± SD Compering to the rate of glucose uptake in DMSO treated L6 myotubes (100%)
5	5	24	138.14 ± 4.23
6	50	5	279.55 ± 17.12
7	50	24	**315.53 ± 21.56**
8	50	24	159.39 ± 12.34
9	25	24	156.34 ± 11.24
12	100	24	No effect
13	40	5	173.35 ± 16.53
14	100	24	No effect
15	25	5	154.15 ± 11.44
19	25	5	124.76 ± 6.24

the maximal effect on glucose uptake is bolded

GLUT4 was measured by detection of the myc epitope in an extracellular loop of the transporter (60). The total cell content of GLUT4 in L6 myotubes was not altered by **7** (Fig. 1g). Yet, it significantly increased GLUT4 abundance in on the cellular surface in a dose-dependent manner following 24-h incubation (Fig. 1g). The minimal effective concertation of **7** in increasing GLUT4 abundance in the plasma membrane was obtained at 5 μM (1.4-fold), and the maximal effect (nearly 2 fold) at 25 μM, a similar concertation that was required to induce the maximal effect on the rate of glucose uptake (Fig. 1a).

The effects of **7** on AMPK may involve activation of LKB1, which is a major upstream kinase that phosphorylates AMPK α-subunit at Thr172 (74). Therefore, the potential of **7** to activate LKB1 was investigated. Figure 2a, b shows that **7** increased dose-dependently Ser428 phosphorylation in LKB1 in L6 myotubes within 24 h of incubation. Specifically, 10 μM of **7** increased the phosphorylation nearly by 30%, whereas 25 μM produced maximal phosphorylation (≈80%). Interestingly, these data also show that insulin induced significant (2-fold) LKB1 phosphorylation in L6 myotubes; however, the consequences of this activation are unclear.

Insulin-mediated and AMPK-dependent augmentation of glucose transport in skeletal muscle requires the activation of the protein AS160, which is involved in the regulation of the translocation of GLUT4-rich vesicles to the plasma membrane of myotubes (75,76). We therefore tested the extent of Thr642 phosphorylation in AS160 in L6 myotubes treated with **7**. Figure 2c, d shows that AS160 was significantly phosphorylated (≈5-fold) already after 1-h incubation with 25 μM of **7**, and this effect persisted up to 5 h, dropping to nearly 2-fold at 24 h. Iinterestingly, the effect of **7** on Thr642 phosphorylation in AS160 was significantly stronger than that of insulin in the same experimental system. To further test the cellular kinase activity of AMPK in **7**-treated cells we measured its ability to phosphorylate its selective down-stream target Acetyl-CoA carboxylase (ACC) (77). Figure 2e, f shows that **7** increased Ser79 phosphorylation of ACC in dose-dependent manner. A maximal 4-fold augmentation of the phosphorylation was observed with 15 μM of compound **7** after 24 h of incubation. These findings suggest that **7** augments glucose transport in myotubes by activating the LKB1-AMPK-AS160 pathway.

Fig. 1 Compound **7** augments glucose uptake in L6 myotubes by activating AMPK. (**a**) Dose response analysis: L6 myotubes were maintained in αMEM containing 23.0 mM glucose for 48 h, then washed and incubated with the same fresh medium supplemented with the indicated concentrations of **7** or DMSO (0.1%, *v*/*v*) for additional 24 h. At the end of incubation the cells were taken for the standard [^{3}H]dGlc uptake assay. The basal rate of dGlc uptake with DMSO (0.1%, v/v)-treated L6 myotubes (7.34 ± 0.59 nmol/mg protein/min) was taken as 100%. (**b**) Time course analysis: L6 myotubes were incubated with 25.0 μM of **7** or DMSO for the indicated periods of time and assayed for [^{3}H]dGlc uptake. The basal rate of [^{3}H]dGlc uptake at zero time (4.11 ± 0.33 nmol/mg protein/min) was taken as 100%. (**c**) Dose response analysis of AMPK activation: L6 myotube cultures were treated with DMSO or with increasing concentrations of **7** or with 0.25 M sorbitol (S, positive control). After 24 h whole cell lysates were prepared and Western blot analyses performed with antibodies against p-172ThrAMPKα and AMPKα. Representative blots are shown. Level of total AMPKα was used for the p-172ThrAMPKα band density normalization for each condition. (**d**) A graphical representation of the bands density shown in panel C. (**e**) Time dependent activation of AMPK: L6 myotube cultures were treated with DMSO or with 25 μM of **7** or 0.25 M sorbitol and taken for analysis at the indicated time points. Whole cell lysates were prepared and Western blot analyses were performed with antibodies against p-172ThrAMPKα and AMPKα. Representative blots are shown. The level of total AMPK (t-AMPK) was used for the p-172ThrAMPKα band density normalization per each treatment. (**f**) A graphical representation of the bands density shown in the panel E. (**g**) Dose response analysis of the effect of **7** on the plasma membrane abundance of GLUT4myc: Myotubes expressing GLUT4myc were treated with increasing concentrations of **7**, 0.25 M of sorbitol (S) or DMSO for 24 h. At the end of the incubation the cultures were taken for immunodetection of surface GLUT4myc as described in the Experimental Section. The upper panel is shown a reprehensive blot of total level of GLUT4 in L6 lysates, whereas the lower panel shows plasma membrane-associated GLUT4myc. The level of GLUT4myc in DMSO- treated myotubes was taken as 100%. *$p < 0.05$, in comparison to the respective controls. $n = 5$–6.

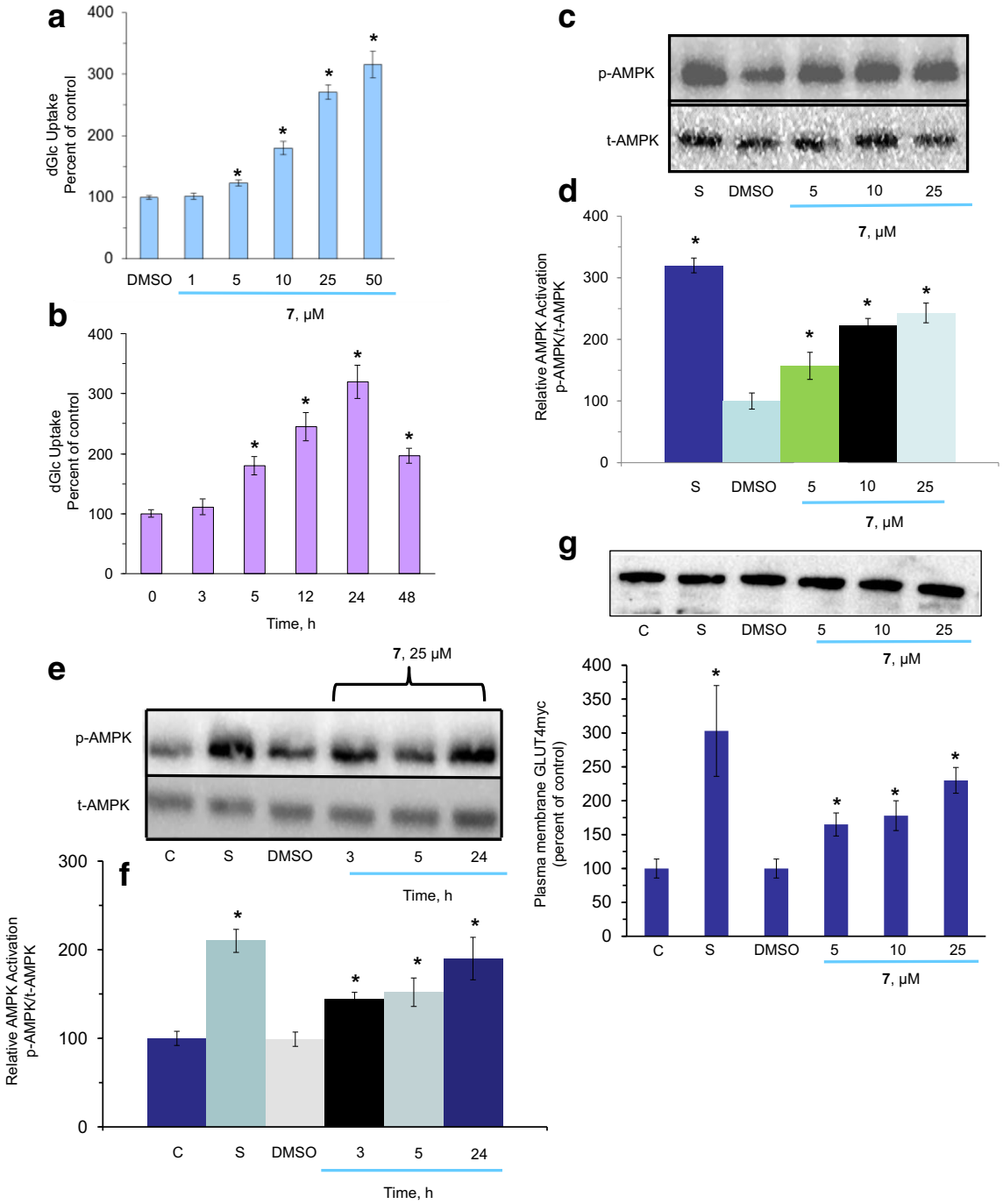

To further investigate the role of AMPK in this pathway, the impact of silencing of the expression of AMPKα2 subunit with shRNA was studied (78). This treatment reduced significantly the cellular content of the protein (Fig. 3a). The finding that **7** was unable to produce any glucose uptake stimulatory effect under this treatment (Fig. 3b) attests to the critical role of AMPK in mediating the biological effect of **7** in L6 myotubes.

Since both insulin and **7** increased the plasma membrane content of GLUT4, albeit with different time-courses, we investigated whether **7** could also employ the insulin transduction pathway to exert this effect. The phosphorylation of Ser437 in Akt/PKB, the key protein in the insulin transduction pathway, was determined (79). Figure 3c, d shows that insulin, but not **7**, induced significant Akt/PKB phosphorylation in treated myotubes.

Studies on the role of AMPK activators in augmenting insulin secretion led us to investigate whether **7** could dually augment glucose uptake in skeletal muscle cells and stimulate insulin secretion from beta cells. The possible effect of **7** on insulin

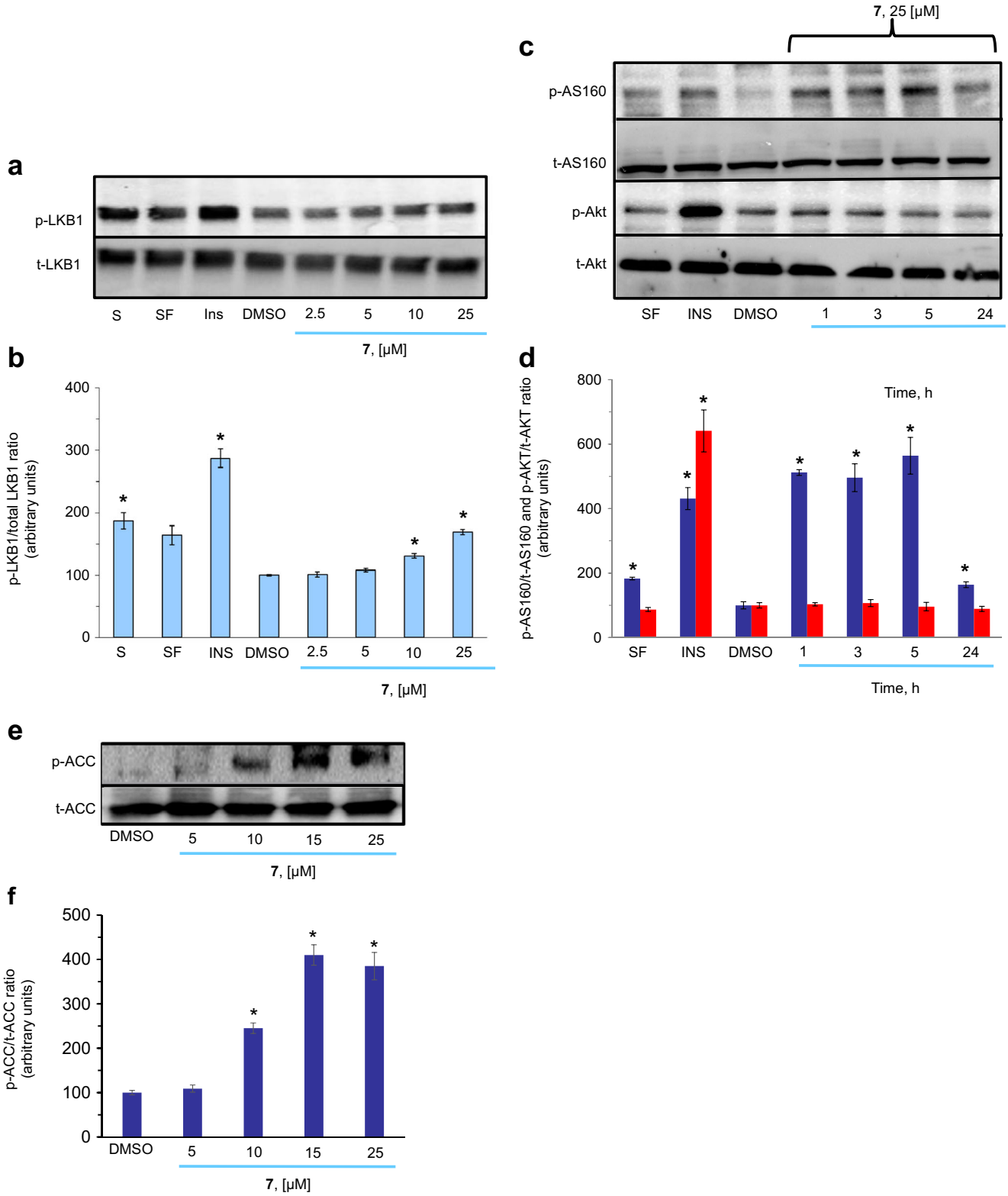

secretion from INS-1E beta-cells was investigated under static incubations (65). It exhibited significant dose-dependent stimulatory effect on the insulin secretory capacity of the cells after 24 h of incubation (Fig. 4a). Half-maximal and maximal effects of **7** on GSIS were obtained with 5 and 10 μM, respectively. Importantly, the stimulatory effects of **7** at 10 and 25 μM were similar. Noteworthy, the basal rate of insulin secretion (at 3.3 mM glucose) was unaltered in the presence of **7** and the

◀ **Fig. 2** Effects of **7** on LKB1, ACC, AS160 and Akt/PKB in L6 myotubes. (**a**) Dose response analysis of the effect of **7** on the level of p-428SerLKB1: L6 Myotubes were treated as described in the Fig. 1c. Insulin (100 nM, INS) was introduced during the last 20 min of incubation. Myotubes which received insulin were kept 5 h before the insulin addition in free serum medium (SF). Sorbitol (0.25 M, S) was used as a positive control. Whole cell lysates were prepared and taken for Western blot analysis. The level of total LKB1 (t-LKB1) was used for the p-428SerLKB1 band density normalization per each treatment. (**b**) Graphical presentation of the bands density of the image shown in A. (**c**) Time course analysis of the effect of **7** on the levels of p-Thr642AS160 and p-Ser437AKT/PKB in L6 myotubes: Myotubes were incubated with 25 μM of **7** or the vehicle [DMSO, 0.1% (v/v)] for the indicated periods of time. The levels of total As160 (t-AS160) and total Akt/PKB (t-AKT/PKB) were used for the p-Thr642AS160 and p-Ser437AKT/PKB band density normalization per each treatment. (**d**) Graphical presentation of the bands density of the image shown in C. Band density of the DMSO-treated cells was taken as 100%. Blue columns represent p-AS160 and the red represent p-AKT/PKB levels. (**e**) Dose response analysis of the effect of **7** on the phosphorylation level of ACC: L6 myotubes treated with increased concentrations of **7** and DMSO (0.1%). Whole cell lysates were prepared and taken for Western blot analysis of total or phosphorylated p-Ser79ACC and total ACC. The p-Ser79ACC bands density was normalized to amount of total ACC (t-ACC) for each treatment. (**f**) Graphical presentation of the bands density of the image shown in E. *$p < 0.05$, in comparison to DMSO treatment, n = 5–7.

total intracellular content of insulin was not affected by **7** (Fig. 4b). The compound was not toxic for INS-1E beta-cells at these concentrations (SI Fig. 1B).

We then asked whether **7**-induced increases of GSIS in INS-1E also involved AMPK activation like in L6 myotubes. Indeed it significantly increased AMPK phosphorylation (Thr172) in a dose-dependent manner; maximal effect was observed with 10 µM (Fig. 4c, d). Figure 4e, f shows the time-dependent effect of **7** on AMPK phosphorylation: maximal effect (2-fold) was observed after 12 h of incubation, decreasing slightly at 24 h. In addition, **7** induced LKB1 phosphorylation (Ser428) in beta-cells at 24-h incubations in a dose-dependent manner. The minimal effective concentration of **7** was 2.5 µM (50% increase) and at 25 µM led to 3-fold effect (Fig. 5a, b). Compound **7** also induced ACC phosphorylation (Ser79) within 24 h of incubation, as shown in Fig. 5c, d; at 25 µM it led to 8-fold augmentation in the phosphorylation level of ACC. Thus, the effect of **7** on beta-cell LKB1/AMPK pathway was similar to that observed in muscle cells, albeit with a somewhat greater efficacy.

Collectively, these data show that **7**, increased glucose uptake in L6 myotubes in a non-insulin-dependent manner and augmented GSIS from beta-cells through AMPK activation. This bi-functionality of **7** represents an interesting class of potential antidiabetic compounds that may reduce blood glucose levels by correcting the two main defects in T2D, the reduced glucose uptake in skeletal muscles, and the impeded insulin secretion from beta-cells.

The druggability of **7** was then investigated. Two basic metabolic *in vitro* pharmacokinetic tests were conducted. First, possible inhibitory effects of **7** on "human ether-à-

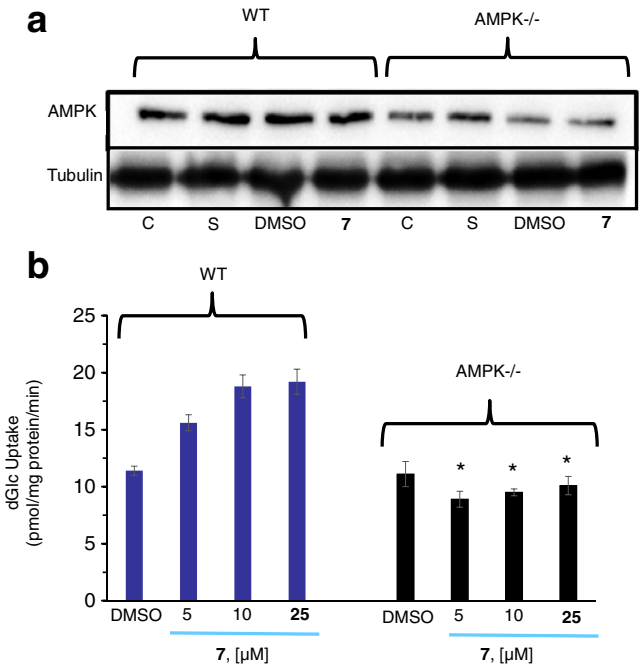

Fig. 3 AMPKα2 silencing diminishes the effect of **7** in L6 myotubes. (**a**) Silencing of AMPK α2: Wild type (WT) cells and shRNA AMPKα2-treated (AMPK−/−) L6 myotubes were maintained in αMEM containing 23 mM glucose for 24 h, then washed and incubated with the same fresh medium supplemented with 25 μM of **7** or DMSO (0.1%, v/v) for 24 h. Sorbitol (0.25 M, S) was added for 2 h. Whole cell lysates were prepared and Western blot analyses were performed with antibodies against AMPKα2 and tubulin (loading control), according to manufacturer's protocols. Representative blots are shown. (**b**) Dose response analysis of **7** on glucose uptake in Wild type (WT) cells and shRNA AMPKα2-treated (AMPK−/−) L6 myotubes: The cultures were treated with **7** (5, 10 and 25 μM) and DMSO as described above. At the end of incubation both types of myotubes were taken for the standard [^{3}H]dGlc uptake assay. The basal rate of dGlc uptake with DMSO (5.71 ± 0.51 nmol/mg protein/min) was taken as 100%. *$p < 0.05$, in comparison to the respective controls, $n = 3$.

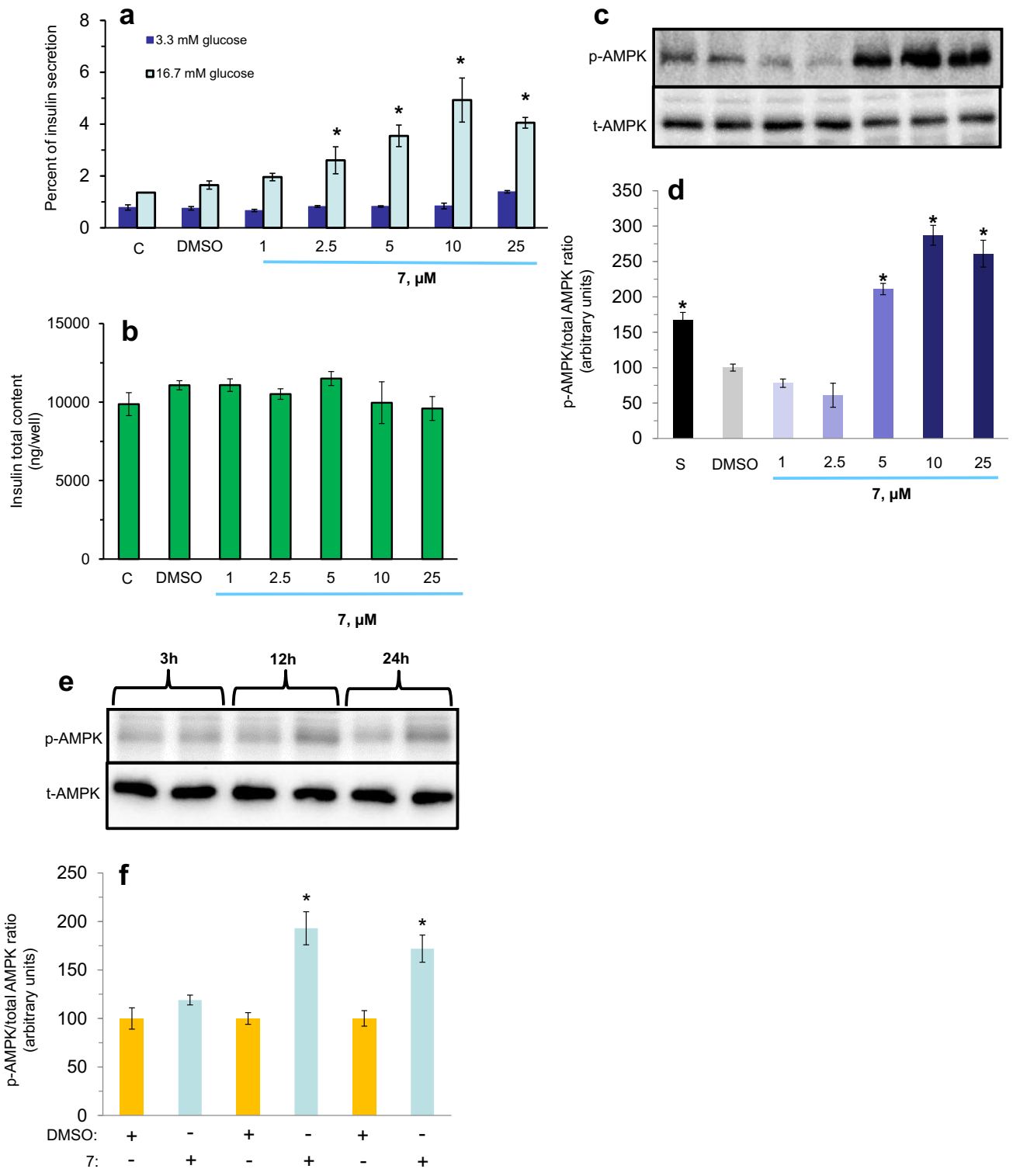

go-go"-related gene channels (hERG) and P450 enzymes were tested. The human hERG potassium channels conduct the rapid component of the delayed rectifier potassium current, which is crucial for repolarization of cardiac action potentials (80). Blocking hERG channels by drugs and drug candidates can lead to action potential prolongation, lengthening of the QT interval and an increased risk for "torsade de pointes" arrhythmias and sudden death (80). Thus, the possible inhibition of hERG channels is one of the negative features of any drug candidate

◀ **Fig. 4** Compound **7** augments insulin secretion from INS-1E beta cells. (**a**) Dose response analysis: The cells were grown and treated with the indicated concretions of **7** for 24 h. The cells were then washed and taken for the standard GSIS, as described in the "Experimental Section". (**b**) Lack of the effect of **7** on the total insulin content: Similarly treated cells as in A were washed and lysed and the whole cells insulin levels were determined as described under "Experimental Section". (**c**) Dose response analysis of AMPK activation by **7**: INS-1E cells were treated with DMSO (0.1%, v/v), with increasing concentrations of **7** or with 0.25 M of sorbitol (S) for 24 h. Whole cell lysates were then prepared and Western blot analyses were performed with antibodies against p-172ThrAMPKα and AMPKα, according to manufacturer's protocols. Representative blots are shown. Level of total AMPK (t-AMPK) was used for the p-172ThrAMPKα band density normalization for each treatment. The density the band of DMSO treated cells was taken as 100%. (**d**) Graphical presentation of the bands density of the image shown in C. (**e**) Compound **7** activates AMPK in INS-1E time-dependently: INS-1E cells were grown and treated with 25 μM of **7** or DMSO (0.1% v/v). Whole cell lysates were prepared at the indicated times and taken for Western blot analysis for p-Thr172AMPK and total AMPK t-AMPK. The density of the total AMPK t-AMPK bands was used for normalization of the p-Thr172AMPK signal. The density of DMSO treated-cells at 3 h was taken as 100%. (**f**) Graphical presentation of the bands density of the image shown in E. Representative blots are shown * $p < 0.05$, in comparison to DMSO treatment, $n = 4$.

which must be avoided (81). The ability of compound **7** to bind to hERG was investigated using a fluorescence polarization assay. SI Table 1 shows no evidence for 7-mediated hERG inhibition at the tested concentrations..

Cytochromes P450 (CYPs) form the most important family of enzymes that catalyze a broad spectrum of oxidation-derived biotransformation of xenobiotics (and numerous drugs among them) (82). In humans, approximately 110 genes encode this battery of P450 enzymes. Interestingly, among all CYPs the enzymes belonging to group 1, 2 and 3 metabolize the vast majority of drugs (82). The effect of **7** on five most relevant P450 isotypes, 2C19, 1A2, 2C9, 2D6 and 3A4 was tested using the P450-Glo™ Assay Systems for drug metabolism and toxicity (Table 2). The data indicates that **7** exhibited a relatively high level (≈80%) of inhibition of 2C19 at 5 μM. Two additional CYPs: 1A2, 2C9 were inhibited by ≈45%. The activity the 2D6 and 3A4 isotypes was not strongly suppressed by **7**. Very strong inhibition of only one CYP out of five tested is considered encouraging in the process of drug design and optimization. Interestingly, many approved drugs such as fluoxetine (83), omeprazole (84), cimetidine (85) and isoniazid (86) are potent 2C19 inhibitors.

Finally, the possible toxicity of compound **7** in human non-cancer cells was investigated. Human monocytes and HEK293 cells were exposed to compound **7** (50 μM) for 24 h. Trypan blue exclusion test or MTT were used to evaluate possible toxic effect of **7** on cells viability. In both types of cells, compound **7** dids not shown any effect on the viability of the cells (SI Fig. 1C, D).

CONCLUSIONS

This study shows that 6-(1,3-dithiepan-2-yl)-2-phenylchromane (**7**), a novel phenylchromane derivative,

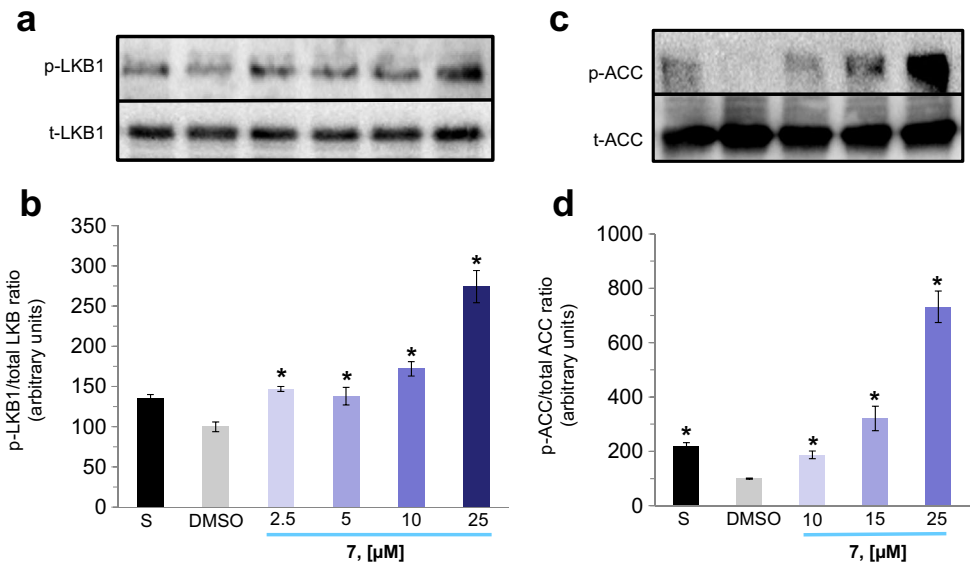

Fig. 5 Effects of **7** on LKB1 and ACC in INS-1E β-cells. (**a**) Dose response effect of **7** on the level of p-LKB1 Ser428: The cells were treated as described in the legend to Fig. 4a. Sorbitol (0.25 M, S) was used as a positive control. Whole cell lysates were used for Western blot analysis. The levels of total LKB1 (t-LKB1) and p-428SerLKB1 were determined with corresponding antibodies according to manufacturer's protocols. The level of t-LKB1 was used for the p-428SerLKB1 band density normalization for each treatment. (**b**) Graphical presentation of the bands density of the image shown in A: DMSO treated cells were taken as 100% (**c**) Dose response analysis of the effect of **7** on the level of Ser79-ACC phosphorylation. The cells were treated as described above and whole cells lysates were used for Western blot analysis. The levels of total ACC (t-ACC) and p-79SerACC were determined with selective antibodies according to manufacturer's protocols. The level of t-ACC was used for the p-79SerACC band density normalization for each treatment. DMSO-treated cells were taken as 100%. (**d**) Graphical presentation of the bands density of the image shown in C. Representative blots are shown. *$p < 0.05$, in comparison to DMSO treatment, $n = 4$.

Table 2 Percent of inhibition of P450 enzymes by compound 7 in concertation of 5 **μ**M

CYP	% of inhibition ± SD
1A2	53.2 ± 1.3
2C9	57.1 ± 9.3
2C19	78.8 ± 3.3
2D6	21.9 ± 2.7
3A4	34.7 ± 14.5

increased the rate of glucose uptake in L6 myotubes under hyperglycemic conditions at pharmacologically relevant concentration. Moreover, **7** augmented glucose-stimulated insulin secretion from beta-cells. Both activities were mediated via the activation of LKB1-AMPK pathway. Finally, predicted pharmacokinetic properties investigated using *in vitro* methods showed druggable properties, which make it a suitable candidate for future development. We anticipate that this bifunctionality of **7** will make it a lead compound in the development of a novel class of antidiabetic drugs.

ACKNOWLEDGMENTS AND DISCLOSURES

We thank Dr. Rachel Hertz, Department of Human Nutrition and Metabolism, The Hebrew University Faculty of Medicine, Jerusalem, Israel, for providing us the lentivirus shRNA-AMPK construct. We thank Ms. Duha Fahham for her technical help. This study was supported partly by a Bar-Ilan University new faculty grant (A.G), by Diab R&D (France) for (E.C., A.G. and S.S.) and grants from the Applied Research Program A of the Hebrew University, and the Israel Science Foundation of The Israel Academy of Sciences and Humanities (to S.S). S. Sasson is member of the David R. Bloom Center for Pharmacy and in Chair Dr. Adolf and Klara Brettler Center for Research in Molecular Pharmacology and Therapeutics. S.S. is the Adolf D. and Horty Storch Chair in Pharmaceutical Sciences, Faculty of Medicine, The Hebrew University of Jerusalem.

REFERENCES

1. Rojasand LB, Gomes MB. Metformin: an old but still the best treatment for type 2 diabetes. Diabetol Metab Syndr. 2013;5:6.
2. Consoli A, Gomis R, Halimi S, Home PD, Mehnert H, Strojek K, *et al.* Initiating oral glucose-lowering therapy with metformin in type 2 diabetic patients: an evidence-based strategy to reduce the burden of late-developing diabetes complications. Diabetes Metab. 2004;30: 509–16.
3. Jensenand TE, Richter EA. Regulation of glucose and glycogen metabolism during and after exercise. J Physiol. 2012;590:1069–76.
4. Rana S, Blowers EC, Natarajan A. Small molecule adenosine 5′-monophosphate activated protein kinase (AMPK) modulators and human diseases. J Med Chem. 2015;58:2–29.
5. Karlssonand HK, Zierath JR. Insulin signaling and glucose transport in insulin resistant human skeletal muscle. Cell Biochem Biophys. 2007;48:103–13.
6. Richterand EA, Hargreaves M. Exercise, GLUT4, and skeletal muscle glucose uptake. Physiol Rev. 2013;93:993–1017.
7. Klip A, Schertzer JD, Bilan PJ, Thong F, Antonescu C. Regulation of glucose transporter 4 traffic by energy deprivation from mitochondrial compromise. Acta Physiol (Oxf). 2009;196:27–35.
8. Ojuka EO. Role of calcium and AMP kinase in the regulation of mitochondrial biogenesis and GLUT4 levels in muscle. Proc Nutr Soc. 2004;63:275–8.
9. Hardie DG. AMPK: positive and negative regulation, and its role in whole-body energy homeostasis. Curr Opin Cell Biol. 2015;33:1–7.
10. Kyriakis JM. At the crossroads: AMP-activated kinase and the LKB1 tumor suppressor link cell proliferation to metabolic regulation. J Biol. 2003;2:26.
11. Jiang SJ, Dong H, Li JB, Xu LJ, Zou X, Wang KF, *et al.* Berberine inhibits hepatic gluconeogenesis via the LKB1-AMPK-TORC2 signaling pathway in streptozotocin-induced diabetic rats. World J Gastroenterol. 2015;21:7777–85.
12. Xie Z, Ding SQ, Shen YF. Silibinin activates AMP-activated protein kinase to protect neuronal cells from oxygen and glucose deprivation-re-oxygenation. Biochem Biophys Res Commun. 2014;454:313–9.
13. Yang Y, Zhao Z, Liu Y, Kang X, Zhang H, Meng M. Suppression of oxidative stress and improvement of liver functions in mice by ursolic acid via LKB1-AMP-activated protein kinase signaling. J Gastroenterol Hepatol. 2015;30:609–18.
14. Zaks I, Getter T, Gruzman A. Activators of AMPK: not just for Type II diabetes. Future Med Chem. 2014;6:1325–53.
15. Cameronand KO, Kurumbail RG. Recent progress in the identification of adenosine monophosphate-activated protein kinase (AMPK) activators. Bioorg Med Chem Lett. 2016;26:5139–48.
16. Giordanettoand F, Karis D. Direct AMP-activated protein kinase activators: a review of evidence from the patent literature. Expert Opin Ther Pat. 2012;22:1467–77.
17. Sliwinskaand A, Drzewoski J. Molecular action of metformin in hepatocytes: an updated insight. Curr Diabetes Rev. 2015;11: 175–81.
18. Zhou JY, Xu B, Li L, New Role A. for an Old Drug: Metformin Targets MicroRNAs in Treating Diabetes and Cancer. Drug Dev Res. 2015;76:263–9.
19. Foretz M, Guigas B, Bertrand L, Pollak M, Viollet B. Metformin: from mechanisms of action to therapies. Cell Metab. 2014;20:953–66.
20. Cohen G, Riahi Y, Alpert E, Gruzman A, Sasson S. The roles of hyperglycaemia and oxidative stress in the rise and collapse of the natural protective mechanism against vascular endothelial cell dysfunction in diabetes. Arch Physiol Biochem. 2007;113:259–67.
21. Cameron KO, Kung DW, Kalgutkar AS, Kurumbail RG, Miller R, Salatto CT, *et al.* Discovery and Preclinical Characterization of 6-Chloro-5-[4-(1-hydroxycyclobutyl)phenyl]-1H-indole-3-carboxylic Acid (PF-06409577), a Direct Activator of Adenosine Monophosphate-activated Protein Kinase (AMPK), for the Potential Treatment of Diabetic Nephropathy. J Med Chem. 2016;59:8068–81.
22. Hsu MH, Savas U, Lasker JM, Johnson EF. Genistein, resveratrol, and 5-aminoimidazole-4-carboxamide-1-beta-D-ribofuranoside induce cytochrome P450 4F2 expression through an AMP-activated protein kinase-dependent pathway. J Pharmacol Exp Ther. 2011;337:125–36.
23. Benziane B, Bjornholm M, Lantier L, Viollet B, Zierath JR, Chibalin AV. AMP-activated protein kinase activator A-769662 is an inhibitor of the Na(+)-K(+)-ATPase. Am J Physiol Cell Physiol. 2009;297:C1554–66.

24. Mirguet O, Sautet S, Clement CA, Toum J, Donche F, Marques C, *et al.* Discovery of Pyridones As Oral AMPK Direct Activators. ACS Med Chem Lett. 2013;4:632–6.
25. Ojukaand EO, Goyaram V. Mechanisms in exercise-induced increase in glucose disposal in skeletal muscle. Med Sport Sci. 2014;60:71–81.
26. Krishan S, Richardson DR, Sahni S. Adenosine monophosphate-activated kinase and its key role in catabolism: structure, regulation, biological activity, and pharmacological activation. Mol Pharmacol. 2015;87:363–77.
27. Miglianico M, Nicolaes GA, Neumann D. Pharmacological Targeting of AMP-Activated Protein Kinase and Opportunities for Computer-Aided Drug Design. J Med Chem. 2016;59:2879–93.
28. Kone M, Pullen TJ, Sun G, Ibberson M, Martinez-Sanchez A, Sayers S, *et al.* LKB1 and AMPK differentially regulate pancreatic beta-cell identity. FASEB J. 2014;28:4972–85.
29. Swisa A, Granot Z, Tamarina N, Sayers S, Bardeesy N, Philipson L, *et al.* Loss of Liver Kinase B1 (LKB1) in Beta Cells Enhances Glucose-stimulated Insulin Secretion Despite Profound Mitochondrial Defects. J Biol Chem. 2015;290:20934–46.
30. Sun G, Tarasov AI, McGinty JA, French PM, McDonald A, Leclerc I, *et al.* LKB1 deletion with the RIP2.Cre transgene modifies pancreatic beta-cell morphology and enhances insulin secretion *in vivo*. Am J Physiol Endocrinol Metab. 2010;298:E1261–73.
31. Fu A, Robitaille K, Faubert B, Reeks C, Dai XQ, Hardy AB, *et al.* LKB1 couples glucose metabolism to insulin secretion in mice. Diabetologia. 2015;58:1513–22.
32. Granot Z, Swisa A, Magenheim J, Stolovich-Rain M, Fujimoto W, Manduchi E, *et al.* LKB1 regulates pancreatic beta cell size, polarity, and function. Cell Metab. 2009;10:296–308.
33. Fu A, Ng AC, Depatie C, Wijesekara N, He Y, Wang GS, *et al.* Loss of Lkb1 in adult beta cells increases beta cell mass and enhances glucose tolerance in mice. Cell Metab. 2009;10:285–95.
34. Fu A, Eberhard CE, Screaton RA. Role of AMPK in pancreatic beta cell function. Mol Cell Endocrinol. 2013;366:127–34.
35. Langelueddecke C, Jakab M, Ketterl N, Lehner L, Hufnagl C, Schmidt S, *et al.* Effect of the AMP-kinase modulators AICAR, metformin and compound C on insulin secretion of INS-1E rat insulinoma cells under standard cell culture conditions. Cell Physiol Biochem. 2012;29:75–86.
36. da Silva Xavier G, Leclerc I, Varadi A, Tsuboi T, Moule SK, Rutter GA. Role for AMP-activated protein kinase in glucose-stimulated insulin secretion and preproinsulin gene expression. Biochem J. 2003;371:761–74.
37. Sun G, Tarasov AI, McGinty J, McDonald A, da Silva Xavier G, Gorman T, *et al.* Ablation of AMP-activated protein kinase alpha1 and alpha2 from mouse pancreatic beta cells and RIP2.Cre neurons suppresses insulin release *in vivo*. Diabetologia. 2010;53:924–36.
38. Ryu GR, Lee MK, Lee E, Ko SH, Ahn YB, Kim JW, *et al.* Activation of AMP-activated protein kinase mediates acute and severe hypoxic injury to pancreatic beta cells. Biochem Biophys Res Commun. 2009;386:356–62.
39. Beall C, Watterson KR, McCrimmon RJ, Ashford ML. AMPK modulates glucose-sensing in insulin-secreting cells by altered phosphotransfer to KATP channels. J Bioenerg Biomembr. 2013;45:229–41.
40. Matsuda T, Takai T, Suzuki E, Kanno A, Koyanagi-Kimura M, Asahara S-i, *et al.* Regulation of Pancreatic β Cell Mass by Cross-Interaction between CCAAT Enhancer Binding Protein β Induced by Endoplasmic Reticulum Stress and AMP-Activated Protein Kinase Activity. PLoS One. 2015;10:e0130757.
41. Wang K, Sun Y, Lin P, Song J, Zhao R, Li W, *et al.* Liraglutide Activates AMPK Signaling and Partially Restores Normal Circadian Rhythm and Insulin Secretion in Pancreatic Islets in Diabetic Mice. Biol Pharm Bull. 2015;38:1142–9.
42. Pasternak L, Meltzer-Mats E, Babai-Shani G, Cohen G, Viskind O, Eckel J, *et al.* Benzothiazole derivatives augment glucose uptake in skeletal muscle cells and stimulate insulin secretion from pancreatic beta-cells via AMPK activation. Chem Commun (Camb). 2014;50:11222–5.
43. Beall C, Piipari K, Al-Qassab H, Smith MA, Parker N, Carling D, *et al.* Loss of AMP-activated protein kinase α2 subunit in mouse β-cells impairs glucose-stimulated insulin secretion and inhibits their sensitivity to hypoglycaemia. Biochem J. 2010;429:323–33.
44. Gruzman A, Elgart A, Viskind O, Billauer H, Dotan S, Cohen G, *et al.* Antihyperglycaemic activity of 2,4:3,5-dibenzylidene-D-xylose-diethyl dithioacetal in diabetic mice. J Cell Mol Med. 2012;16:594–604.
45. Gruzman A, Shamni O, Ben Yakir M, Sandovski D, Elgart A, Alpert E, *et al.* Novel D-Xylose Derivatives Stimulate Muscle Glucose Uptake by Activating AMP-Activated Protein Kinase α. J Med Chem. 2008;51:8096–108.
46. Meltzer-Mats E, Babai-Shani G, Pasternak L, Uritsky N, Getter T, Viskind O, *et al.* Synthesis and mechanism of hypoglycemic activity of benzothiazole derivatives. J Med Chem. 2013;56:5335–50.
47. Gottlieb HE, Kotlyar V, Nudelman A. NMR chemical shifts of common laboratory solvents as trace impurities. J Org Chem. 1997;62:7512–5.
48. La Regina G, Diodata D'Auria F, Tafi A, Piscitelli F, Olla S, Caporuscio F, *et al.* 1-[(3-Aryloxy-3-aryl)propyl]-1H-imidazoles, New Imidazoles with Potent Activity against Candida albicans and Dermatophytes. Synthesis, Structure-Activity Relationship, and Molecular Modeling Studies. J Med Chem. 2008;51:3841–55.
49. Hodgetts KJ. A stereocontrolled route to 2-substituted chromans. Tetrahedron Lett. 2000;41:8655–9.
50. Hodgetts KJ. Inter- and intramolecular Mitsunobu reaction based approaches to 2-substituted chromans and chroman-4-ones. Tetrahedron. 2005;61:6860–70.
51. Ongand BS, Chan TH. A simple method of dithioacetalization and dithioketalization. Synth Commun. 1977;7:283–6.
52. Kimura M, Hamakawa T, Hanabusa K, Shirai H, Kobayashi N. Synthesis of Multicomponent Systems Composed of One Phthalocyanine and Four Terpyridine Ligands. Inorg Chem. 2001;40:4775–9.
53. Handrickand GR, Atkinson ER. Potential antiradiation drugs. III. 2-Amino-2-alkyl-1,3-propanedithiols and 3-amino-4-mercapto-1-butanol. J Med Chem. 1966;9:558–62.
54. Zhong W, Tang Y, Zampella G, Wang X, Yang X, Hu B, *et al.* A rare bond between a soft metal (FeI) and a relatively hard base (RO-, R = phenolic moiety). Inorg Chem Commun. 2010;13:1089–92.
55. Munder A, Moskovitz Y, Redko B, Levy AR, Ruthstein S, Gellerman G, *et al.* Antiproliferative Effect of Novel Aminoacridine-based Compounds. Med Chem. 2015;11:373–82.
56. Shimanovich U, Munder A, Azoia NG, Cavaco-Paulo A, Gruzman A, Knowles TP, *et al.* Sonochemically-induced spectral shift as a probe of green fluorescent protein release from nano capsules. RSC Adv. 2014;4:10303–9.
57. Suckow AT, Zhang C, Egodage S, Comoletti D, Taylor P, Miller MT, *et al.* Transcellular neuroligin-2 interactions enhance insulin secretion and are integral to pancreatic beta cell function. J Biol Chem. 2012;287:19816–26.
58. Sanderson RJ, Shepperdson RT, Vatter AE, Talmage DW. Isolation and enumeration of peripheral blood monocytes. J Immunol. 1977;118:1409–14.
59. Eckshtain-Levi M, Lavi R, Yufit DS, Daniel B, Green O, Fleker O, *et al.* A versatile water-soluble chelating and radical scavenging platform. Chem Commun (Camb). 2016;52:2350–3.
60. Shapira R, Rudnick S, Daniel B, Viskind O, Aisha V, Richman M, *et al.* Multifunctional cyclic D,L-α-peptide architectures stimulate non-

insulin dependent glucose uptake in skeletal muscle cells and protect them against oxidative stress. J Med Chem. 2013;56:6709–18.
61. Zatara G, Hertz R, Shaked M, Mayorek N, Morad E, Grad E, *et al.* Suppression of FoxO1 activity by long-chain fatty acyl analogs. Diabetes. 2011;60:1872–81.
62. Cohen G, Riahi Y, Shamni O, Guichardant M, Chatgilialoglu C, Ferreri C, *et al.* Role of lipid peroxidation and PPAR-delta in amplifying glucose-stimulated insulin secretion. Diabetes. 2011;60: 2830–42.
63. Li XQ, Andersson TB, Ahlstrom M, Weidolf L. Comparison of inhibitory effects of the proton pump-inhibiting drugs omeprazole, esomeprazole, lansoprazole, pantoprazole, and rabeprazole on human cytochrome P450 activities. Drug Metab Dispos. 2004;32:821–7.
64. Niwa T, Shiraga T, Takagi A. Effect of antifungal drugs on cytochrome P450 (CYP) 2C9, CYP2C19, and CYP3A4 activities in human liver microsomes. Biol Pharm Bull. 2005;28:1805–8.
65. Mori T, Sawada Y, Oku A. Ring-expansion of thioacetal ring via bicyclosulfonium ylide. Effect Of protic nucleophile on ylide intermediate J Org Chem. 2000;65:3620–5.
66. Cui Z, Chen X, Lu B, Park SK, Xu T, Xie Z, *et al.* Preliminary quantitative profile of differential protein expression between rat L6 myoblasts and myotubes by stable isotope labeling with amino acids in cell culture. Proteomics. 2009;9:1274–92.
67. Wertheimer E, Sasson S, Cerasi E. Regulation of hexose transport in L8 myocytes by glucose: possible sites of interaction. J Cell Physiol. 1990;143:330–6.
68. Itani SI, Saha AK, Kurowski TG, Coffin HR, Tornheim K, Ruderman NB. Glucose autoregulates its uptake in skeletal muscle: involvement of AMP-activated protein kinase. Diabetes. 2003;52: 1635–40.
69. Ben-Yakir M, Gruzman A, Alpert E, Sasson S. Glucose transport regulators. Current Medicinal Chemistry-Immunology. Endocr Metab Agents. 2005;5:519–27.
70. Shamni O, Cohen G, Gruzman A, Zaid H, Klip A, Cerasi E, *et al.* Regulation of GLUT4 activity in myotubes by 3-O-methyl-d-glucose. Biochim Biophys Acta. 2017;1859:1900–10.
71. Shamni O, Cohen G, Gruzman A, Zaid H, Klip A, Cerasi E, *et al.* Supportive data on the regulation of GLUT4 activity by 3-O-methyl-D-glucose. Data Brief. 2017;14:329–36.
72. Furtado LM, Somwar R, Sweeney G, Niu W, Klip A. Activation of the glucose transporter GLUT4 by insulin. Biochem Cell Biol. 2002;80:569–78.
73. Chiu TT, Jensen TE, Sylow L, Richter EA, Klip A. Rac1 signalling towards GLUT4/glucose uptake in skeletal muscle. Cell Signal. 2011;23:1546–54.
74. Kottakisand F, Bardeesy N. LKB1-AMPK axis revisited. Cell Res. 2012;22:1617–20.
75. Cao S, Li B, Yi X, Chang B, Zhu B, Lian Z, *et al.* Effects of exercise on AMPK signaling and downstream components to PI3K in rat with type 2 diabetes. PLoS One. 2012;7:e51709.
76. Deshmukh AS, Hawley JA, Zierath JR. Exercise-induced phosphoproteins in skeletal muscle. Int J Obes (Lond) 32 Suppl. 2008;4: S18–23.
77. Hardieand DG, Pan DA. Regulation of fatty acid synthesis and oxidation by the AMP-activated protein kinase. Biochem Soc Trans. 2002;30:1064–70.
78. Ross FA, MacKintosh C, Hardie DG. AMP-activated protein kinase: a cellular energy sensor that comes in 12 flavours. FEBS J. 2016;283:2987–3001.
79. Mackenzieand RW, Elliott BT. Akt/PKB activation and insulin signaling: a novel insulin signaling pathway in the treatment of type 2 diabetes. Diabetes Metab Syndr Obes. 2014;7:55–64.
80. Thomas D, Karle CA, Kiehn J. The cardiac hERG/IKr potassium channel as pharmacological target: structure, function, regulation, and clinical applications. Curr Pharm Des. 2006;12:2271–83.
81. Pierson JB, Berridge BR, Brooks MB, Dreher K, Koerner J, Schultze AE, *et al.* A public-private consortium advances cardiac safety evaluation: achievements of the HESI Cardiac Safety Technical Committee. J Pharmacol Toxicol Methods. 2013;68:7–12.
82. Zangerand UM, Schwab M. Cytochrome P450 enzymes in drug metabolism: regulation of gene expression, enzyme activities, and impact of genetic variation. Pharmacol Ther. 2013;138:103–41.
83. Sager JE, Lutz JD, Foti RS, Davis C, Kunze KL, Isoherranen N. Fluoxetine- and norfluoxetine-mediated complex drug-drug interactions: *in vitro* to *in vivo* correlation of effects on CYP2D6, CYP2C19, and CYP3A4. Clin Pharmacol Ther. 2014;95:653–62.
84. Quinn DI, Nemunaitis J, Fuloria J, Britten CD, Gabrail N, Yee L, *et al.* Effect of the cytochrome P450 2C19 inhibitor omeprazole on the pharmacokinetics and safety profile of bortezomib in patients with advanced solid tumours, non-Hodgkin's lymphoma or multiple myeloma. Clin Pharmacokinet. 2009;48:199–209.
85. Furuta S, Kamada E, Suzuki T, Sugimoto T, Kawabata Y, Shinozaki Y, *et al.* Inhibition of drug metabolism in human liver microsomes by nizatidine, cimetidine and omeprazole. Xenobiotica. 2001;31:1–10.
86. Wen X, Wang J-S, Neuvonen PJ, Backman JT. Isoniazid is a mechanism-based inhibitor of cytochrome P450 1A2, 2A6, 2C19 and 3A4 isoforms in human liver microsomes. Eur J Clin Pharmacol. 2002;57:799–804.